EXPERIMENTAL INVESTIGATION OF SHEAR INFLOW OVER AN AIRFOIL

A DISSERTATION

Submitted in partial fulfillment of the

requirements for the award of the degree

of

MASTER OF TECHNOLOGY

in

MECHANICAL ENGINEERING

(With specialization in Thermal Engineering)

By

MUKESH KUMAR SAHU

DEPARTMENT OF MECHANICAL & INDUSTRIAL ENGINEERING

INDIAN INSTITUTE OF TECHNOLOGY ROORKEE

ROORKEE-247667 (INDIA)

JUNE, 2019

INDIAN INSTITUTE OF TECHNOLOGY

ROORKEE

CANDIDATE'S DECLARATION

I hereby certify that the work which is being presented in the thesis entitled **"EXPERIMENTAL INVESTIGATION OF SHEAR INFLOW OVER AN AIRFOIL"** in partial fulfilment of the requirements for the award of the Degree of "Master of Technology" and submitted in the Department of Mechanical and Industrial Engineering of the Indian Institute of Technology Roorkee is an authentic record of my own work carried out during the period from July, 2018 to June, 2019 under the supervision of Dr. Sushanta Dutta, Associate Professor, Department of Mechanical and Industrial Engineering, Indian Institute of Technology Roorkee.

The matter presented in this thesis has not been submitted by me for the award of any other degree of this or any other institute.

Date: **(MUKESH KUMAR SAHU)**

Place: Roorkee

CERTIFICATE

This is to certify that the above statement made by the candidate is correct to the best of my knowledge.

Dr. Sushanta Dutta

Associate Professor

MIED

IIT ROORKEE

ACKNOWLEDGEMENT

I wish to express my sincere and earnest gratitude and thanks to my supervisor Dr.Sushanta Dutta, Associate Professor, Department of Mechanical and Industrial Engineering, IIT Roorkee for providing me this valuable research topic, their guidance, valuable suggestions, constructive criticism and continuous support with patience and encouragement throughout the period of this research work. His warm personal approach and painstaking efforts in going through the manuscript are gratefully acknowledged.

I express my sincere thanks to Dr. B.K. Gandhi, Professor and Head of the Department of Mechanical and Industrial Engineering for his encouragement and overall supervision in bringing out this report.

I am very thankful to my family, research scholars, Mr. Kamal Raj Sharma, Mr. Vikas Sharma and Mr. Tarachand Mourya and all of my friends for their never ending encouragement in bringing out this project report to the form which it is now.

Place: Roorkee

Date:

Mukesh Kumar Sahu

M.Tech (Thermal Engineering)

Enroll. No. 17541008

MIED, IIT Roorkee

Abstract

Flow over an airfoil at low Reynolds is a challenging research area which has many engineering applications that attracts the interests of the scientific community. There is shear layer transition and wake transitions involved in this regime which can directly effects the aerodynamic characteristics of the airfoil. Study of these transition phenomena may help in controlling the flow better as well as it will aide to the understanding of the subject. Apart from this, the uniform free stream flow over an airfoil has been extensively studied in the literature. Effects of uniform shear flow on the load characteristics of airfoil and wake structure of flow over the airfoil is not well known yet since the literature is scarce in this field of research. There are many parts of the aircraft which are subjected to shear flow like airfoil area near the propellers and jet engines and root the wings. Moreover, while landing and take-off, the aircraft wings have to generate massive lift force and minimum drag force under the shear flow and even during cruising, the aircraft has to face turbulence caused by shear flow near mountains. The present study takes this research problem and tries to reveal the flow physics involved in the low Reynolds regime comparing the flow kinematics and dynamics of uniform inflow and uniform shear inflow to a NACA0012 airfoil. Hotwire anemometer setup (Constant temperature type) is used in the present study to characterize the flow over the airfoil. The experiments are performed in a low turbulence level subsonic wind tunnel. The study reveal that the uniform shear inflow enhances the momentum flux of the boundary layer thus makes it able to bear adverse pressure gradients at High angles of attack. The separation is delayed in the case of uniform shear inflow over the airfoil with respect to uniform free stream inflow. The vortex shedding is observed for high angles of attack in uniform free stream inflow case whereas, for uniform shear inflow case it is observed for only 12^{o} angle of attack. The time-averaged drag coefficient calculation using momentum balance method reveals that airfoil bears fewer drag in the case of uniform shear inflow than uniform freestream inflow for nearly all angles of attack and for both the Reynolds numbers used in the study.

Table of contents

List of Figures

List of Tables

Chapter 1 Introduction

In today's modern world with the time, the demand of energy is increasing day by day. On one hand there is a search for an alternating source of energy and on the other hand, research work is going on to reduce the energy consumption. Aerodynamics is an important field of science which greatly effects the efficiency of any moving object. Aerodynamics is the study of interaction of fluid with the object having relative motion. It is used in automobile industry, aerospace, wind power industry. Today's modern era of technology is inclined towards producing compact machines and equipment. One such technology is Micro air vehicles (MAV's) and macro Unmanned air vehicles (UAV's) which are used in a combat operation or surveillance missions (example-drones). In such operations, the compactness of machine is necessary to prevent it to be detected by the enemy. MAV's fly at a lower Reynolds number, $Re \leq 10^5$ while Normal aircraft cruise above, $Re \geq 10^6$. Extensive studies have been done in high Re range but comparatively fewer studies have been done in the $Re \leq 10^5$. Study of wing operating in the range of $Re \leq 10^5$ is an emerging field in the past decade. Research tells that for high Re, wings have higher aerodynamic performance but for a range of $Re \leq 10^5$, their aerodynamic performance decreases. So at low Re air vehicles requires more power due to the weak performance of its wings. One reason behind this weak performance is that at low Re, shear layers formed over the airfoil surface are laminar in nature. These shear layers do not have the energy to counter adverse pressure gradient hence start to separate, this phenomenon is called laminar separation. This results in increasing the drag and reducing the lift. The study of this laminar separation theory are done by authors Gad-el-Hak (2001), Jones et al. (2018), Lissaman P.B.S. (1983), Carmichael B.H. (1981).

Shear layers gain more momentum from the flow on the upper surface. Because of that the momentum of shear layers increases hence this increased momentum dominates the adverse pressure gradient separated shear layer attach to the surface of the airfoil. The gap between the separation and reattachment point is called the laminar separation bubble. When adverse pressure gradient increases this bubble collapses and leads to a rapid reduction in lift. Authors Muller and Batill (1982), Hatman and Wang (1999) has done the study of separation bubble formation and have inferred that after gaining momentum from the upper fluid, shear layers reattach back to the airfoil surface having turbulent nature called turbulent boundary layer. For Re of 10^4 - 10^5 turbulent boundary layer and size of the separation bubble increases than the size of the separation bubble at low Re. As the angle of attack increases, this separation bubble moves towards the leading edge. The turbulence in the inflow greatly effects the performance

of airfoil. Aeroplanes fly normally in the smooth flow situation but in specific situation like dust, dust storm or storm, turbulence intensity (TI) of air increases which strongly effect the performance of wings. Muller T.J et al. (1983) performed experiment which shows that the behaviour of NACA 0012 on the Re of 1, 50,000 with turbulence intensity of 0.3% is different from the behaviour obtained when the turbulence was set to the 0.07. Watkins S. et al. (2009) has done experiment with a flat plate with Re of 75,000. They studied the effect of a range of turbulence intensities varied from 1.2% to 12.6% on the drag and lift of plate. They concluded that as TI increases stall angle increases. Tsuchiya et al. (2013) have done an investigation with a range of TI from 0.9% to 1.5% in the flow for Re of 11,000 to 47,000. They have varied angle of attack from -5º to 20º. To change the TI different space having grids or mesh screens were used. As the turbulence intensity increases in Re 4×10^4 the drag coefficient decreases from 0º to 12º but for higher angle, the effect of TI seems negligible.

Mesh screens are also used in various literature to generate the shear or a gradient flow in the wind tunnel test section. Most of the study has been done with airfoil having uniform inflow but very few studies have been done on the airfoil facing non-uniform inflow or uniform shear flow. There are many practical situations where airfoil wings are not subjected to the uniform flow. When aircraft takes off air flow over wings is not uniform due to the shear effect of the wind. A similar situation happens when the aircraft lands. Passing of the aeroplanes near mountain, case of heavy rainfall are similar examples of shear flow. In marine application like tides, the current is the case of uniform flow. The rotor blades operate in the wake zone generated by neighbouring blades similarly the propeller of a ship operates in the wake of another propeller, these are also the case of non-uniform flow.

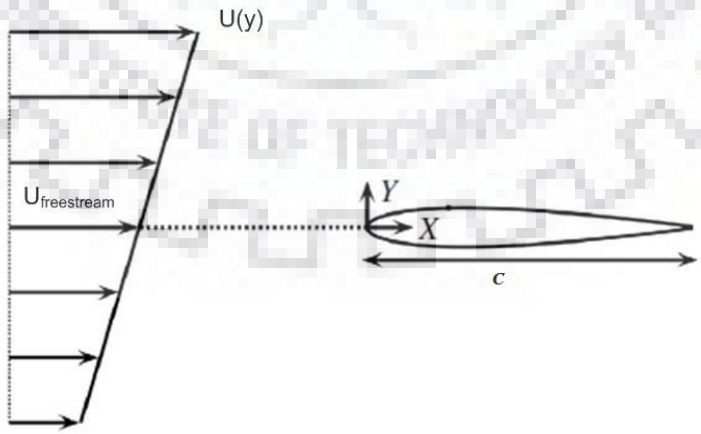

Fig. 1.1 Flow geometry by Tisen (1943)

Where,

c = Chord length of the airfoil

U(y) = velocity

$U_{free\ stream}$ = U = *free* stream velocity

$$K = \frac{c}{U_{free\ stream}} \times \frac{du}{dy}$$

The research related to analysis of aerofoil in the shear flow is firstly done by the Tsien, (1943), who used Joukowsky airfoil. He has given a controlling dimensionless shear parameter (K).

This study tells that due to the presence of shear flow, negative lift is generated at 0º angle of attack which remains zero as in case of uniform inflow case. Hammer et al. (2018) have done the simulation of uniform shear flow over NACA 0012 airfoil. They have done detail comparison of effect of viscous and inviscid effect with the shear parameter. Authors have mentioned that there is an increase in strouhal number when an increase in the shear parameter (K). Payen and Nelson (1985) have done experiments with the uniform shear flow and compared uniform inflow and uniform shear flow over NACA 0018 and result shows as angle of attack increases from 0º to 15º till 5º C_D for shear and uniform flow remains similar and beyond that C_D for uniform inflow is lower than the C_D of shear flow case.

The objective of this work is to design and fabricate aerofoil as well as shear screen to generate the shear flow in a wind tunnel test setup. The dimension wind tunnel is 61×61 cm^2 NACA 0012 Aerofoil is used having chord length of 15 cm and span of 60 cm. The experiments are performed for two free stream velocity of 4.6 m/s and 7.7 m/s corresponds to Reynolds number of (based on chord length) of 4×10^4 and 8×10^4 respectively. Shear parameter (K) used in the work is 0.0162 obtained which is a weak shear and remains constant for both the Reynolds number. This shear zone is throughout the height of cross-section. The effect of shear inflow and uniform inflow is compared in this project.

1.1 Turbulence intensity (TI): Turbulence intensity tells the fluctuating nature of the flow of air. TI hence it is a very important parameter which greatly influences the aerodynamic performance of an airfoil.

$$TI = \frac{u'}{U}$$

Where $u'$is the root mean square of the fluctuation component in all three directions

$$u' = \sqrt{\frac{{u'_x}^2 + {u'_y}^2 + {u'_z}^2}{3}}$$

1.2 Strouhal number (St): It is the dimensionless number which tells the oscillating or fluctuating flow mechanism. It is the dimensionless frequency of the vortex shedding.

$$St = \frac{fc}{U}$$

Where f is the shedding frequency and C is the chord length of the airfoil.

1.3 Airfoil: Aerofoils are the streamline shaped wings which are used in airplanes, MAV's, and turbomachinery. The shape of airfoil is such that the drag force is very small fraction of lift. National Advisory Committee for Aeronautics (NACA) is an international agency who develops different NACA airfoil (4 digit, 5 digit, 6 digit etc.). The following nomenclatures are used for defining the airfoil

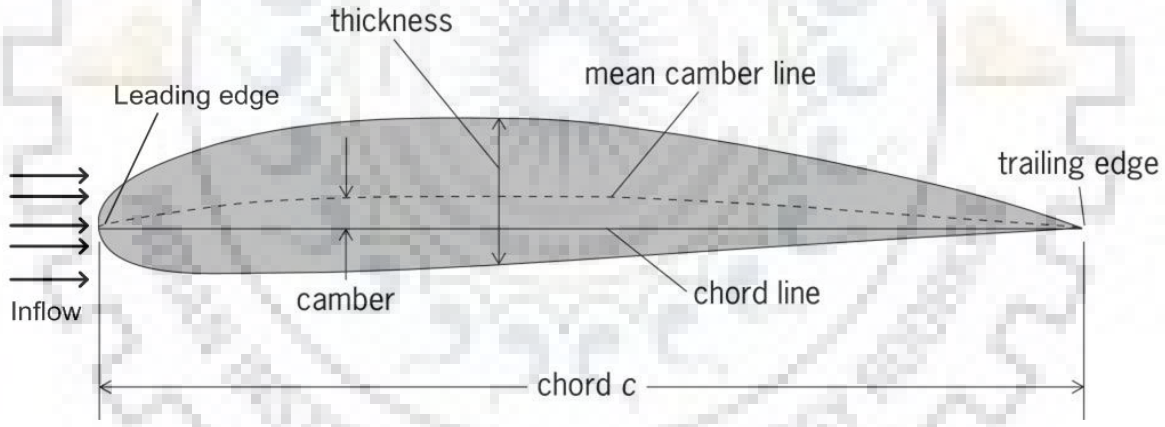

Fig. 1.2 schematic diagram of airfoil (2d).

- The chord C is the distance between the leading edge to trailing edge.
- The length of the airfoil normal to the cross section is called span
- The centre line of the curvature of the cross section of airfoil called mean camber.
- The gap between the camber line and chord is called camber.
- The angle between the direction of inflow and chord line is called angle of attack

- The force acting in the opposite direction of the fluid in flow is called drag force (F_D) and force acting on the airfoil in the perpendicular direction to the flow called lift force (F_L).

1.4 Coefficient of drag (C_D): It is the dimension less number which indicates the drag or resistance offered by the object which is interacting with fluid such that relative motion is not zero between them.

$$C_D = \frac{F_D}{\frac{1}{2}\rho A U^2}$$

Where,

F_D=drag force

ρ= density of fluid

A= resistive drag area

Owen and Zienkiewicz (1957) have proposed the theoretical design to make grids to generate shear flow (2d) in the wind tunnel. They have also done experiments to validate their theoretical design. The grid is made up of 62 of parallel rods having a diameter of 0.125 inches. The spacing between the rods is varying according to theoretical design. This grid is called shear screen. This screen is placed at the beginning of the working section of the wind tunnel. The dimension of the wind tunnel is 20-inch squares and velocity of incoming flow is 75 feet sec^{-1}. These rods provide resistance to the incoming flow results in a change in total pressure difference at large distance downstream side without effecting static pressure near the grid. This leads to shear flow downstream side of the screen in which velocity increases from bottom to top. The authors have chosen a conservative value of shear parameter K_0 as 1.15 and $\frac{\lambda h}{U}$ as 0.45. Though they have also tried $0.2 \leq K_0 \leq 1.0$ and $0.18 \leq \frac{\lambda h}{U} \leq 0.64$. The experiment shows variation in the velocity is 1.12 times of incoming flow to 0.70 times of incoming flow, hence the author called it weak shear. They have also mentioned that due to an undesirable change in the spacing between the rods velocity profile measured varies from the designed one in both along the x and y-direction.

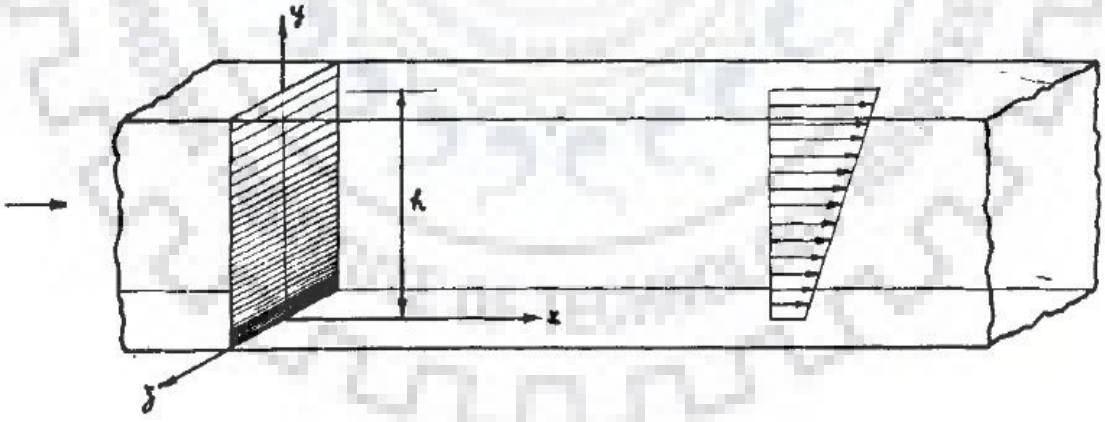

Fig. 2.1 Schematic diagram of flow regime inside tunnel test section (From Owen and Zienkiewicz)

Kwon et al. (1992) performed experiments on the uniform shear flow past circular cylinder were performed in a water tunnel. The image processing technique is used for Flow visualization to capture the flow phenomenon to investigate the vortex shedding. Design and operation of the wind tunnel are taken from Rohr et al. (1988). The tunnel is having a 3mm

shear screen and 5 mm diameter rod to maintain spanwise uniformity in flow. To get uniform shear inlet cross section was made of 19 channels walls, equally spaced stainless steel plates were used. The thickness of each plate is 0.7 mm. flow in each channel is controlled by individual valves. Length of each plate in the direction of flow is 70 cm and flow remains undisturbed from the adjacent layer. To generate uniform shear. The paper shows the variation of Strouhal number with a shear parameter, also shows the variation of C_D with different Re. ($50 \leq Re \leq 160$, $0 \leq K \leq .02$ and B=0.1 and 0.05).

Kang (2005) has numerically investigated two-dimensional uniform shear (laminar) flow over a cylinder where free stream velocity varies linearly with height. The author has used immersed boundary method for simulation of flow over a cylinder. Kim et al. (2001) conducted numerical simulations by systematically varying the Reynolds number, shear rate and blockage ratio in the fairly wide ranges of $50 \leq Re \leq 160$, $0 \leq K \leq .02$ and B=0.1 and 0.05. The governing equations are integrated in time using a second-order semi-implicit fractional-step method: a third-order Runge–Kutta method for the convection terms and a second-order Crank-Nicolson method for the diffusion terms. Velocity profile at the inlet of the condition is $U = U_c + Gy$ where Uc is free stream velocity ($U_{free\ stream}$) It is concluded that the vortex-shedding frequency significantly increased with increasing Reynolds number, while it remained nearly constant or slightly decreased with increasing shear rate. With increasing blockage ratio, on the other hand, the shedding frequency slightly increased all over the ranges of the Reynolds number and shear rate. The mean drag decreased with increasing Reynolds number, and remained nearly constant or slightly decreased with increasing shear rate. With increasing blockage ratio, on the other hand, the mean drag greatly increased. The drag fluctuations greatly increased with increasing Reynolds number or shear rate, but the blockage effect was not so significant. In the case of nonzero shear (K=0), the background vorticity in the free-stream was negative. Therefore, the positive-signed vortices in the near-wake behind the circular cylinder became weakened and elongated, while the negative-signed ones became strengthened and round-shaped.

Hammer et al. (2017) have done a numerical simulation of viscous and inviscid 2d positive shear flow over airfoil NACA0012 at chord length based Re of 1.2×10^4. The shear parameter used are 0 (uniform inflow), 0.5 and 1. O grid meshing is used. To capture the flow physics high-density mesh is used around an airfoil (1.8 times cord length along transverse direction) especially in wake zone downstream side (4 times chord length). Authors have mentioned difficulties to use the positive shear for whole incoming viscus fluid in the inlet

zone. They used three zones for inlet top and bottom as uniform inlet zone and middle is as shear zone. The thickness of the middle zone is such that is does not affect the results. For inviscid fluid, as *K* value increases the coefficient of lift and vortex shedding frequency also increases. An interesting investigation was done by creating a non-uniform boundary layer. Due to positive shear on the top surface velocity is high hence boundary layer formation is thin and on the bottom surface, the boundary layer is thicker due to the lower velocity of the fluid. This difference in boundary layer leads to downward lift due to the difference in displacement thickness.

Laitone (1997) has performed experiment with NACA0012 in the wind tunnel has a facility to change the turbulence intensity from 0.02% to 0.10% through the screen placed in the wind tunnel. Airfoil is mounted on high sensitive two component beam balance having universal joint connects 2 orthogonal balance arms. This is more sensitive than two force balance to measure drag and lift. Authors have done a detailed investigation of the effect of turbulent intensity on drag, lift, coefficient of lift and coefficient of drag at a different angle of attack and Reynolds numbers. The result shows that the increase in turbulence level decreases lifts to drag ratio sudden. The similar drop also obtained for the coefficient of lift. Coefficient of lift jumps near AOA=3º for Re=20700 but for Re=42100 similar trend obtained at AOA=2º. The author has done the interesting investigation by reversing the airfoil i.e. leading edge was facing downstream side and trailing edge was facing upstream side, with this arrangement similar trend of the coefficient of lift but for reversed airfoil C_{Lmax}= 0.67 at AOA=9º and for normal one C_{Lmax}= 0.45 at AOA=4.8º for same Re. Results show C_D decreases when Re increases but this drop is lesser than the Blasius prediction for laminar skin friction drag and more rapid drop than an approximation of turbulent skin friction drag.

Cao et al. (2007) have compared the effect of uniform flow and uniform shear flow over a circular cylinder. The experimental setup consists of wind tunnel having multiple fans controlled individually by computers show that shear flow can be generated with different shear parameter 0, 0.1, 0.2, 0.3. Cylinder diameter of 50mm, 90mm and 110mm are used for the experiment. Result shows mean velocity profile downstream side of the cylinder with uniform inflow and with the uniform shear flow, as shear parameter increase turbulent intensity increases but it is shown that there is not much change in strouhal number. Author has given the explanation that the shear flow has self-adjusting nature hence when shear profile interact with the cylinder the acceleration occurs on low-velocity region to support this comment he shows pressure distribution around the cylinder from 0º to 180º on both top and bottom side

of cylinder and results shows that stagnation point shifts upward side on top surface due to high velocity(coefficient of pressure >1) bottom side pressure is lower till 62º after that on both side pressure remains the same. Pressure difference from 0º to 62º leads the acceleration of flow on the downward direction this creates lift from top (higher velocity) side to bottom (lower velocity side).

Payne and Nelson (1985) have performed experiments in wind tunnel with airfoil NACA 0018 facing uniform shear flow. To generate shear gradient curved but uniform mesh screen was used, which generated shear on the downstream side of the screen. Authors have done details study of the effect of velocity gradient on aerodynamics characteristic pressure coefficient (C_P), drag coefficient (C_D), Lift coefficient (C_L). They mainly focused on the velocity gradient on the turbulent intensity and the effect of turbulence on aerodynamic characteristics. The intensity of uniform inflow and shear flow was 0.1 and 0.5 respectively. Chord length of airfoil was 5.1 inch and span length was 15.4 inch. It was having total 175 pressure ports on total 7 rows 25 port on each row from leading edge to trailing edge. To measure drag, lift two component strain gauge balance with dual flexure system was used. The result shows a detailed comparison of C_P, C_D, C_L, of uniform inflow and shear flow at a different angle of attack from -20º to 20º. For -5º to 5º C_D increases for shear as the angle of attack increases but not much different were seen when changing the angle of attack from -5º to -20º. C_L value remains constant for both type of flow till -7º to 7º and then C_L increases the angle of attack changes from 7º to 15º similar trend obtained when varying from -7º to -15º. The author mentioned that as the effect of shear velocity on aerodynamic characteristic is lesser as compare to turbulent intensity. Turbulent intensity higher for sheared flow than uniform flow.

Ghorbanishohrat et al. (2016) have investigated boundary layer separation oscillating airfoil. To analyse flow separation PIV and infrared thermography technique were used. Wind tunnel dimension was 152.44mm×152.40mm×450mm. 26mm chord length low Reynolds number airfoil was used for the experiment. To give the pitching motion (oscillating motion) and control the orientation of airfoil brushless servo motors was used. For infrared thermography temperature difference between the surface of the airfoil and the incoming free stream was necessary so that the camera can capture temperature contours. To do that thin 0.25mm heating wire was placed on the surface of an airfoil in a zig-zag way for homogenous heating. The result shows that vortex circle diameter =1.5mm and the height of the laminar separation bubble was 1.2mm or 5% - 6% of chord length. As AOA increases till 14º laminar

separation bubble becomes smaller. The authors also have mentioned that since the airfoil dimension is very hence a small vibration significantly effects the PIV results.

Hu and Yang (2008) have done a detailed experimental study on laminar separation over NASA low Re GA (W)-1 airfoil, having chord length of 101mm and Re 70000. They had used PIV for measurement of the flow field in detail. To support pressure on top and bottom of the airfoil are measured for that 43 pressure taps are prepared on airfoil surface at the different chord wise position. Provision is given to rotating the airfoil from 4º to 15º. The result shows that for the lower angle of attack (≤ 8º) there is no flow separation are found over airfoil because of adverse pressure gradient are not dominating the than the kinetic energy of flow but as the angle increases adverse pressure gradient starts dominating and separation starts (8º - 10º). Result of surface pressure measurement shows that as the angle of attack increases 8º to 14º there is a rapid decrement in the upper surface of airfoil near 0-0.3C locations, PIV result complements the same. The lower side of airfoil pressure distribution remains almost similar. Separation bubble height is very small nearly 1% of the chord length hence PIV measure can not reveal the laminar separation bubble. Above 12º when the angle of attack increases the adverse pressure gradient dominates significant leads busting of the separated bubble due to that turbulent attachment does not take place hence rapid drop on lift takes place. It was found from the experiment result that C_L increases almost linearly as the angle of attack increases. Stall takes place at 12º. Authors have also mentioned normalizing turbulent kinetic energy distribution, shows higher kinetic energy zone downstream side of separation bubble which validates the basic fundamental concept that after the separation flow has more capability to resist adverse pressure gradient than laminar flow.

Winslow et al. (2018) have done CFD simulation of uniform in flow over airfoil (NACA 0012, 0009, flat plate airfoil) at a different angle of attack and Reynolds number were varied from 10^4 – 10^5. Authors have focused on the aerodynamic performance of airfoil in lower Reynolds number ($\leq 10^5$). Aerodynamics characteristics of the airfoil are highly sensitive to the lower Re and do not depend upon only Re and geometry of airfoil but also in turbulence nature of inflow. For lower Re aerofoils unlike to the high Re airfoil ($Re \geq 10^6$) there are two phenomenon on airfoil surface first separation bubble forms on upper surface of airfoil which moves towards leading edge when AOA increases and the second one is that other separation bubble formed near trailing edge (near 8º) till the separation of bubble from the upper surface as AOA increases (12º -14º). As Re decreases from 10^5 to 10^4 C_L increases by 46% was recorded. Unlike the high Re in low Re, the lift curve is not linear (up to 10º). Authors also

have done an aerodynamic performance comparison between the flat plate (2% t/c flat plate) and NACA 0012 at different AOA but same Re 2×10^4. It was found that in this Re laminar separation bubble takes place at Airfoil trailing edge and on the upper surface of the airfoil at 5ºof AOA but for flat plate, the bubble was formed at the leading edge and on the upper surface.

Tsuchiya et al. (2013) have performed experiments to study the effect of turbulent intensity on the aerodynamic characteristic of airfoil when airfoil NACA 0012 is subjected to uniform inflow. The experiment had been done in Mars Wind Tunnel having no fans, to maintain wind flow vacuum was created. To maintain the different turbulent intensity in wind, the different turbulent grid was introduced inside the tunnel. Two different wire (diameter of 0.6 mm and 0.9 mm) were used in wired mesh to generate low and high turbulent intensity. The whole experiment was classified in three sections in which there was no mesh grid was placed, second when small wire diameter mesh was placed and third in which large wire diameter mesh was placed. To measure drag and lift two component balance system was installed. To measure the surface pressure over the airfoil, pressure sensitive paint was applied over the surface. It was found from experiments that at angle of attack of 3º to 6º that drag coefficient for Re 25000 was lower than for 47000, this is due to that the turbulence intensity of Re 47000 was lower than the Re 25000. The large difference in the drag coefficient was observed at the angle of attack of 7º to 10º. From the angle of attack of 5º difference in the coefficient of the lift was noticed between grid and no grid condition. Authors experimental results show an increase in turbulence intensity, improve the aerodynamic characteristics of the airfoil by reducing the drag and increasing the lift. In the presence of the wire mesh grid, drag coefficient decreases in all condition and lift coefficient increased near stall and at no angle of attacks.

Muller and Batill (1982) have used experimental approach to investigate the laminar separation transition and turbulent reattachment near the leading edge of NACA 663-018 airfoil. In experiment flow visualization was used in the tunnel. For measurement of drag and lift force, strain gauge balance was installed. Authors also have done a study of the effect of surface roughness and external acoustics excitation on boundary layer separation. In this literature, authors have correlated force measurement with results obtained from flow visualization measurements. Airfoil had a dimension of 0.2489 m of chord and 0.4064m of the span. The wind tunnel was set to produce wind with a velocity of 8-27 m/s with the turbulent intensity of 0.10%. Results show that due to present of roughness on airfoil lift coefficient is higher than the case of a smooth surface (0º - 6º) but for 8º - 11º lift coefficient for the smooth

surface was higher than the rough case. For smooth case 0º- 8º drag coefficient decreases (Re 130000) after that sudden increment was observed from 7º-11º. For rough case unlike to the smooth case coefficient of drag increases continuously from 0º -11º, though rapid increment was observed in drag coefficient from 7º-11º.

Yarusevych et al. (2009) have done a study of the effect of Reynolds number on boundary layer separation, transition in separated shear layer and reattachment. In the experiment NACA 0025 was used, Reynolds number was varied from $5.5\times10^3 \leq Re \leq 210\times10^3$ and angle of attack from 0º to 10º. It was found from the experimental results that when the flow is subjected to adverse pressure gradient flow start to separate from the top surface of airfoil called as a shear layer, this shear layer gain the energy from upper flow region and hence start shear roll up after that this shear layer roll up start to shed with

Yarusevych et al. (2009) have studied the low to medium Reynolds number regime of flow over a NACA 0025 airfoil experimentally. Different angle of attack have also been varied like 0, 5, and 10. CTA and flow visualization experiments revealed the coherent structure involved in the two flow regimes there is a boundary layer separation bubble formed. These two regimes without varied slightly on Re ranges for a different angle of attacks. Laminar to turbulent transition in shear layer is shown using power spectra at the different stream-wise location and through flow visualization photographs. The study showed that the shear layer rollup shed at a fundamental frequency. Shear layer transition has been shown as a subharmonic growth of a fundamental frequency of disturbances. The vortex merging phenomenon owes to this transition. This subharmonic growth and transition become less pronounced as the Re is increased or the angle of attack is decreased.

The study also showed the fundamental frequency (f_0) scaling is a function of Re with different exponents for the two different flow regimes. To characterize the wake vortex structure the spectrum of the v-velocity component is more sensitive to frequency centred activity or periodic activity. The wake seems to be more organized in the first flow regimes i.e. the boundary layer separation without reattachment the vortices seems equidistance from each other thus wake has single characteristic frequency whereas in the regime of separation with the attachment wake seems to irregular implies broadband shedding activity of vortices. The study also showed that the vortex shedding frequency at any angle of attack increases with increase in Re. the vortex shedding frequency also showed linear dependency on Re for two different flow regimes. The author also proposed a universal frequency scaling to collapse the

Strouhal frequency on the previous experimental data of bluff bodies. The vertical distance between two vortexes forming in the near wake (d^*) is taken as the length scale for universal strouhal number. It is the distance between the two local peaks in the rms velocity graph

Hung and Lin (1995) performed experiments on a wing using flow visualization (smoke wire and surface oil flow and CTA). A cantilever wing NACA 0012 having chord length of 30 cm (AR=5) has been experimented in an open circuit wind tunnel. Flow visualization is done using a smoke-wire technique with high-speed photography and video recording. The study showed that vortex shedding at a low angle of attack resembles Von-Karman Vortex Street but not exactly is Von-Karman instability. Four characteristic vortex shedding modes have been revealed in the study namely laminar, transitional, subcritical and supercritical. These modes are closely related to the behaviour of the boundary layer on the suction surface of the airfoil. If the intensity of turbulence amplifies in the wake then the periodicity of the vortex shedding decreases since this enhanced turbulence may break up the large structures in the flow reducing the coherency in the wake. In laminar vortex shedding mode, the shedding frequency varies with the span location as vortices have a lower frequency around the tip and rot compared to the central span area. This phenomenon is more pronounced for higher Reynolds number. For subcritical shedding, no appreciable variation in vortex shedding frequency is observed. The bluff body resembles at a high angle of attack due to which tip vortex is reduced and turbulence transition around the root area has less influence on boundary layer being the reason of this spanwise unmapped vortex shedding frequency.

The vortex shedding at low root angles of attack in the wake region evolves from the shear layer-instabilities, whereas at a high angle of attack bluff body characteristics dominate thus low-frequency vortex shedding is superimposed by high-frequency instability waves,

Chapter 3 Experimental setup

The experiments are performed in horizontal open-loop (non-return) subsonic wind tunnel using Pitot-static tube, Micro Manometer and Hot Wire Anemometer. The experimental facility is installed in the wind simulation lab in Mechanical and Industrial Engineering Department at Indian Institute of Technology Roorkee. All experiments are performed over Airfoil NACA 0012 to see the effect of shear inflow and uniform inflow. In this chapter, the detail of the experimental setup, experimental technique, and instrumentation used in the present study is explained.

3.1 Wind Tunnel

Wind Tunnel can be divided into 5 section Honeycomb section, contraction section, two test section (test section 1, test section 2) and diffuser section shown in figure below.

Honeycomb section made up of square wood section having a dimension of 1.81m×1.80m as shown in figure 3.2. Since with this opening flow is allowed to enter hence flow may have all direction i.e. along the axial length (x-direction) and across the axial length of the tunnel (y and z-direction) hence main function of this tunnel is to reduce the y and z directional nature of flow and allow only x directional flow of tunnel but with least pressure drop. For that honeycomb cells are used. These may be of the shape of square, circular or hexagonal shown in figure 3.1.

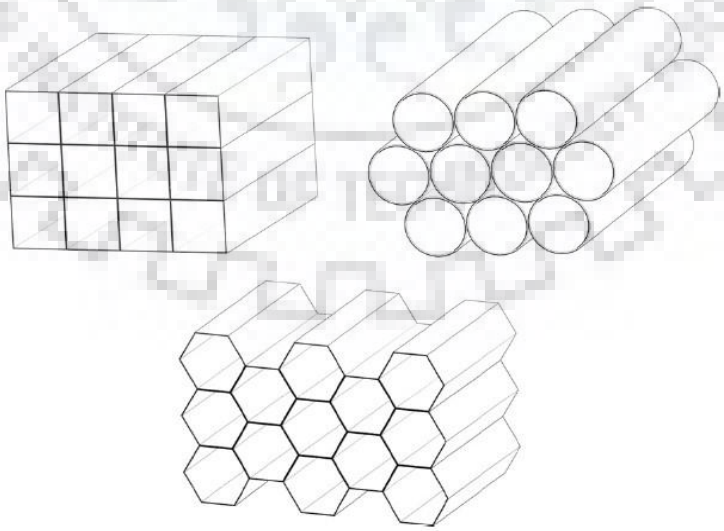

Fig. 3.1 Image of different honeycomb cells, from Kulkarni et al. (2011)

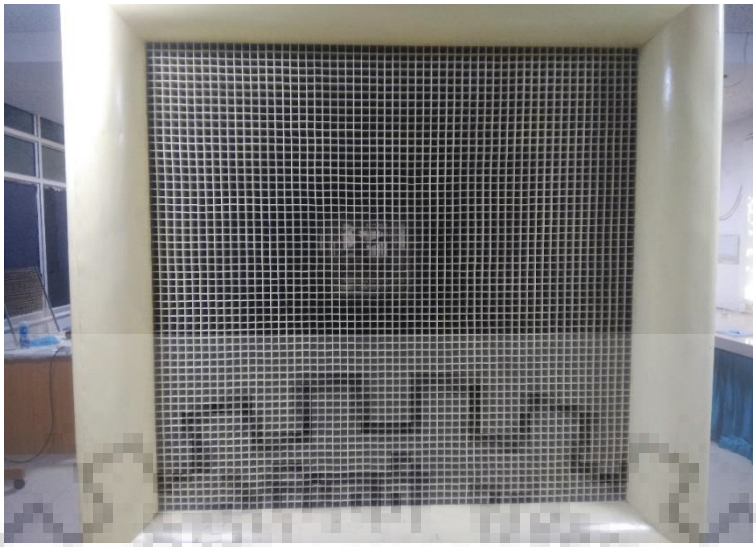

Fig. 3.2 Image of the inlet section of the tunnel (honeycomb)

Fig. 3.3 Image of the honeycomb (zoomed view)

In this tunnel square honeycomb cells are used having a dimension of 3cm×3cm and 10cm in axial flow direction and made up of wood sheet shown in figure 3.3

Settling chamber is connected after honeycomb and contraction cone. The main function of the settling chamber is to reduce the stream wise turbulence of the flow. For that two fine mesh screen are installed in the settling chamber 33.5cm just after the small wooden

square section in the direction of flow. These fine meshes are made up of stainless steel. These fine mesh also reduce the turbulence of inflow.

Fig.3.4 Image of settling chamber

After the settling chamber contraction cone is installed shown in figure 3.5. It is an important section of the wind tunnel. The main function of this section is to accelerate the inflow without increasing the fluctuation in the mean flow and maintaining the parallel streamline in the flow. To avoid the flow separation at the exit of the cone right selection of contraction cone is important. Contraction cone ration is 9:1.

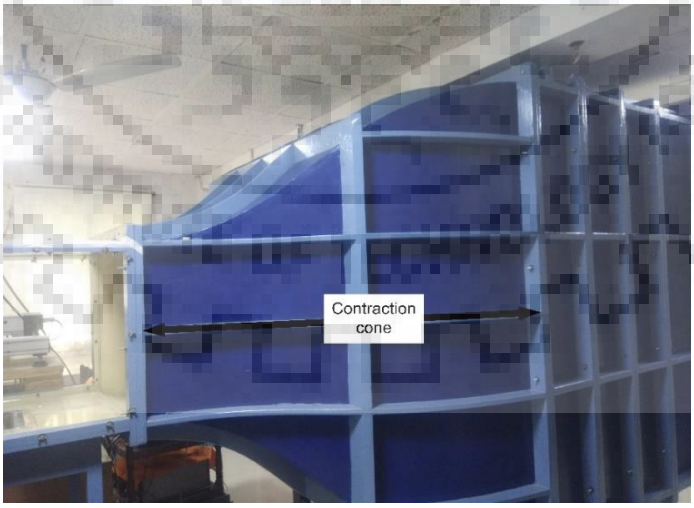

Fig.3.5 Image of contraction cone section of the wind tunnel.

This tunnel consists of two test section (test section 1 and test section 2) in the direction of flow as shown in figure 3.6 and 3.7. Test section 1 has a dimension of 0.61×0.61 m^2 and 1.2 m length in the x-direction. Test section having transparent walls in all 3 side made up of acrylic sheet (thickness 10mm) which are bolted tightly with wood frame and the base is made up of wood and acrylic sheet as shown in figure 3.6. In this section airfoil is placed with a rotating arrangement, for that two holes (6mm and 8mm) are prepared on the two walls. On the one side of the airfoil, the bolt is fixed through adhesive and other side a 5mmhole is prepared. For placing the airfoil inside the tunnel top section is removed and after that bolt, having one side of airfoil is inserted inside the hole and on the other side, a screw is tightened. A set square is stuck on the wall as shown in the figure. To move the hot wire probe in x and y-direction and

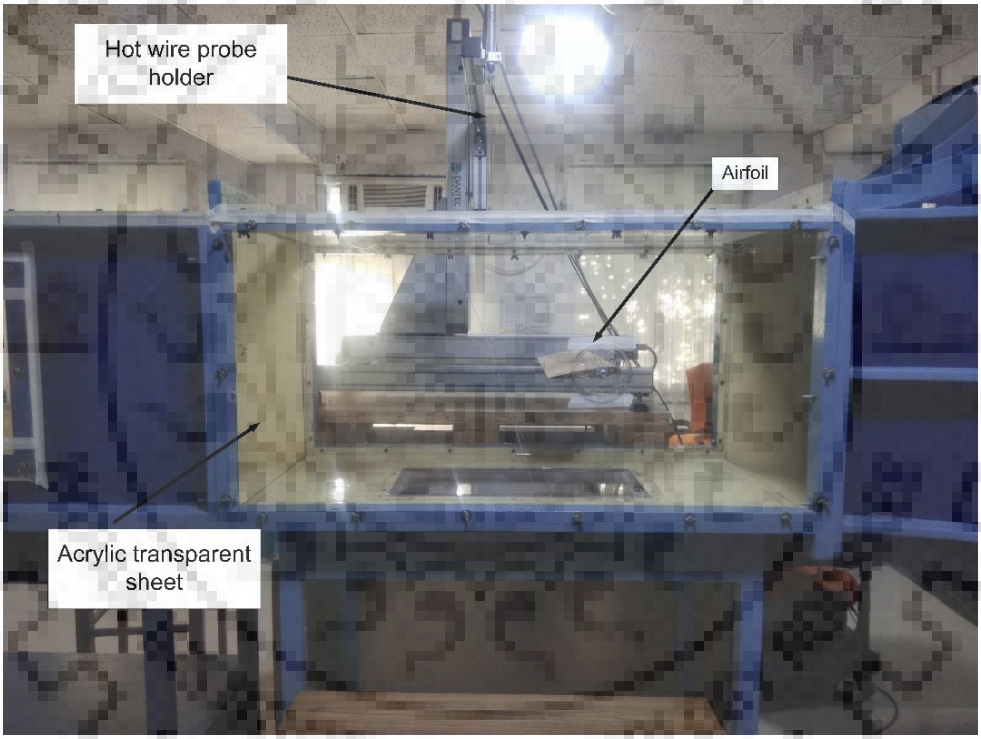

Fig. 3.6 Image of test section 1 having airfoil place inside the tunnel.

1cm wide and 65 cm length slot is made on the top acrylic sheet. Different size of T shape plugs made up of similar acrylic sheet is made to cover the slots and to move the probe location. One T plug is having 8 mm diameter hole, allow hot wire probe to move in the y-direction. In order to prevent the leakage of air from these plugs and other places, proper taping is used.

The test section 2 having the cross-section dimension of 0.61×0.61 m^2 and length 1.52m in the direction of flow. This section is also having similar slots (length 1.2m). Unlike

the test section 1, it is having one top transparent acrylic sheet and other walls are made up of wood. Two side walls are having windows (acrylic) having handles which are bolted tightly on the wood walls. These windows allow to put any object inside the tunnel which effects going to be studied. In this test section, the Pitot-static tube is mounted at different x position and at different depth. To give the depth same hole having plug is used and to give the x position different T plugs are adjusted.

Fig. 3.7 Image of test section 2 of window tunnel

After the test section, a pair of flow simulator is present as shown in figure 3.8. This flow simulator is actually two flat plates called vents which can reduce the cross- section of flow. Hence flow speed can be simulated but in our case, we don't need this simulator hence this simulator are in not working condition

Diffuser section is basically a duct having an increasing cross-section in the direction of flow. The main function of this section is to reduce the velocity of flow and increase the pressure so that at the exit of this section pressure of floe can match to the ambient pressure and air can be removed.

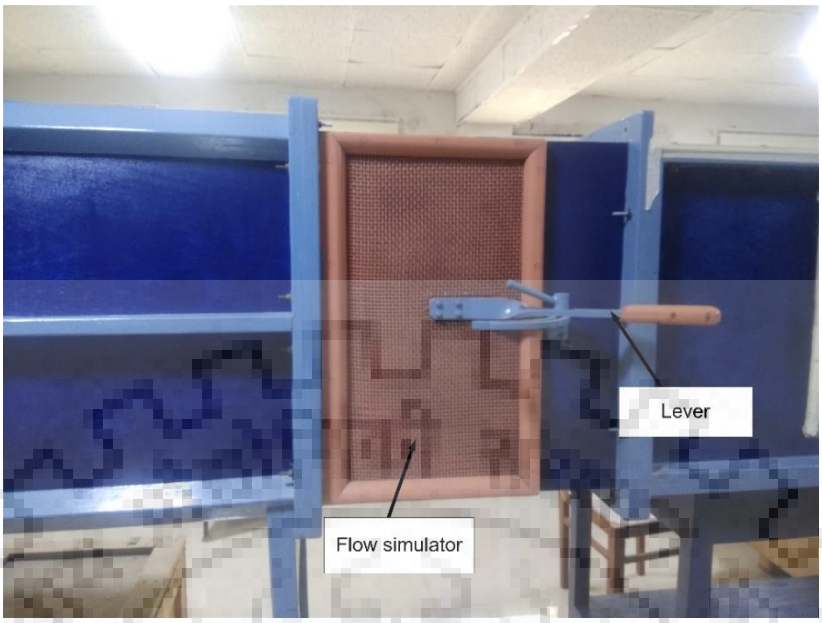

Fig. 3.8 Image of flow simulator section of the wind tunnel.

For smooth flow without turbulence the total diverging angle should be 5º. Maximum pressure recovery is possible up to an angle of 10º, but if the diffuser section length or pressure recovery length is higher than usual length then rule of 5º does not work due to more friction loss. In the present wind tunnel, the diffuser section is having a rectangular inlet and circular outlet at the exit and divergent angle is 4º (figure 3.9).

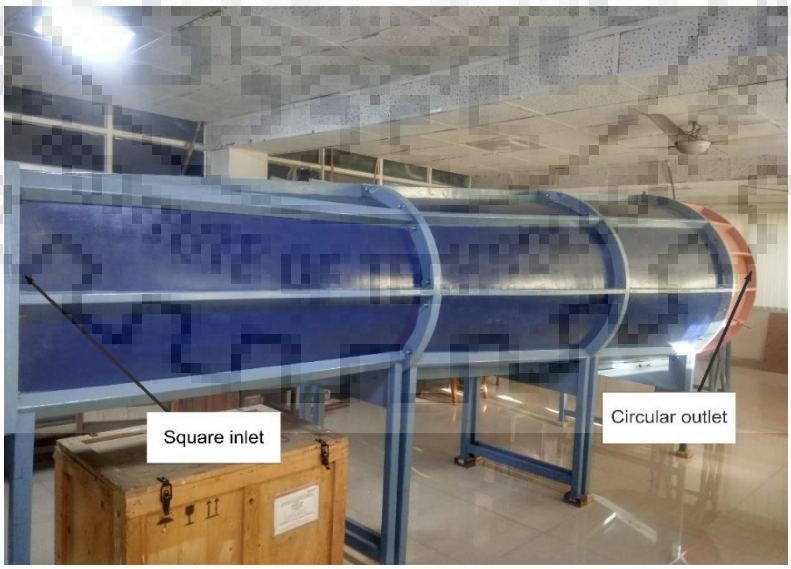

Fig. 3.9 Image of flow diffuser section of the wind tunnel.

The flow in the test section is controlled by a heavy duty fan made up of wood. The shaft of the fan is mounted on bearing housing. In order to avoid the transfer of vibration to the motor to the fan, the shaft of the fan is connected to the motor shaft through the flange coupling. It is connected through the flange coupling to the motor shaft. The maximum speed of the motor (Siemens Company) is 1492 rpm and 20 hp of power (figure 3.10).

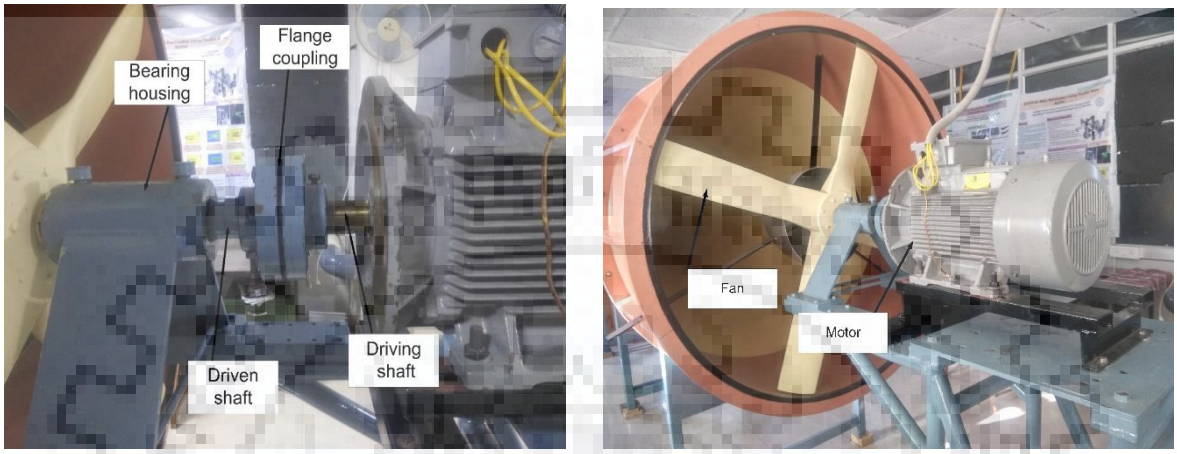

Fig. 3.10 Image of fan and motor

The motor speed is controlled by the 3phase speed controller as shown in figure 3.11

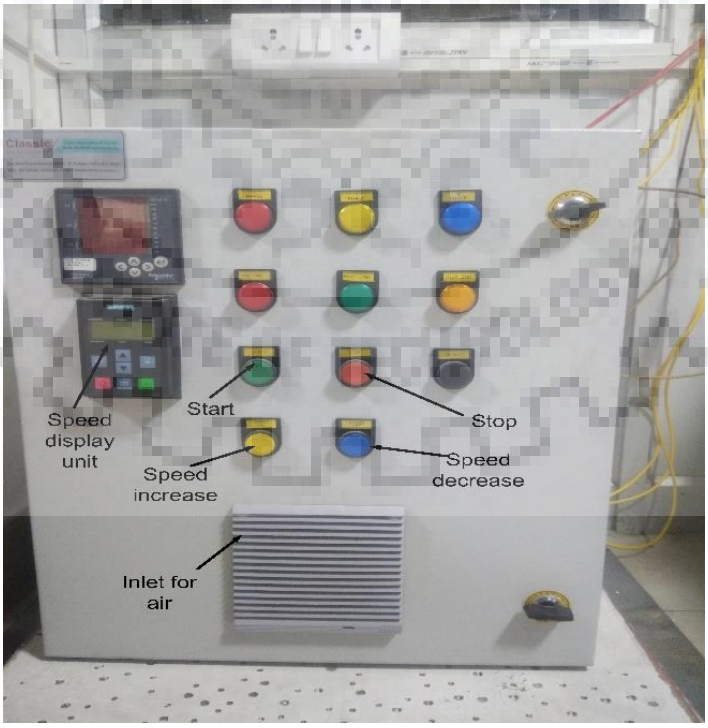

Fig. 3.11 Image of wind tunnel control panel

3.2 NACA 0012 AIRFOIL

Airfoil NACA 0012 is used as the streamlined body to do the study of the effect of uniform inflow and uniform shear flow on the airfoil as shown in figure (). The selection of this NACA coordinate is just because a number of numerical and simulation study has been done with this NACA 0012. Hence to understand the different flow phenomenon around this airfoil is comparatively easy due to the presence of a number of literature available. Coordinates of NACA 0012 is obtained from the internet (www.airfoiltool.com) with the chord length of 15 cm with the close trailing edge. This airfoil coordinate is transported to the Solidworks (version 2016) to get the desired profile with actual scale (1:1) so that it can be used to fabricate the NACA 0012 and chord length is selected 60 cm to avoid the 3d flow in the tunnel as tunnel has a dimension of 61 cm in z-direction. Fabrication of this airfoil is done in the Carpentry shop IIT Roorkee. Deodar (scientific name-Cedrus Deodara) is chosen for the making of airfoil because this wood is relatively soft hence very easy to make any shape with a smoother surface. One major advantage of this wood is that it is light in weight which was the important requirement for the experiment because airfoil has to be fitted on two walls of test section 1 made up of acrylic sheet which cannot bear the high load. After fabrication of airfoil to make surface very smooth polishing with Emery polishing paper (grade5/0). Aspect ratio is 4. While this polishing process was taken care that profile was not affected. To accommodate airfoil inside test section 1, one side of airfoil 8 mm bolt (without head) is fixed with the help of high strength adhesive and on the other side, 6mm hole is prepared. With this bolt and screw, the airfoil is given to the rotation to set the 360^0 protectors is stuck on one the wall of test section 1 as shown in figure 3.12.

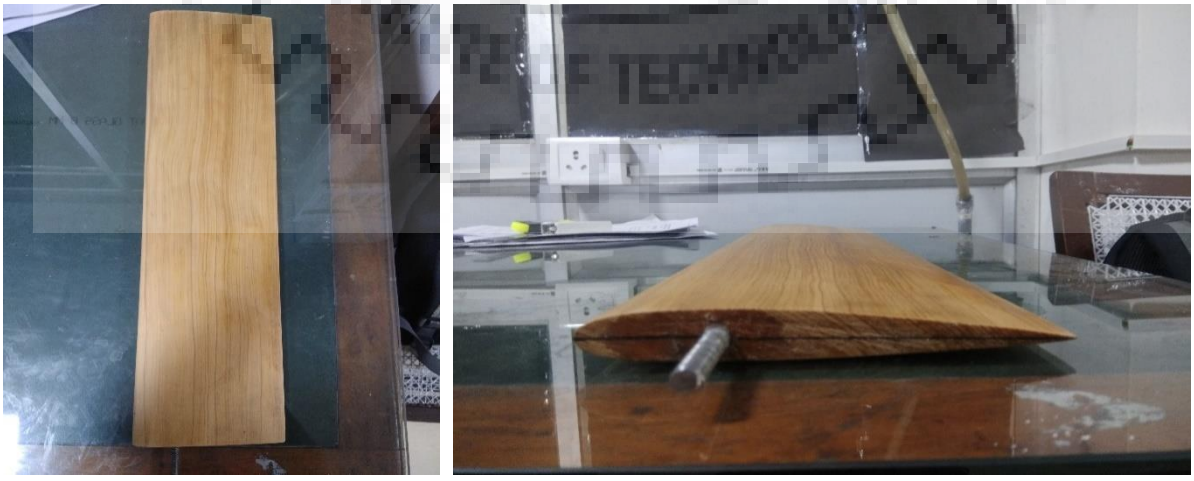

Fig. 3.12 image of airfoil top view (left), side view (right)

Chapter 4 Experimental technique and measurements

In present experimentation, Pitot static tube and hot wire anemometer technique are used to analyse the flow field. The experimental arrangement of the hot wire setup shown in figure 4.1

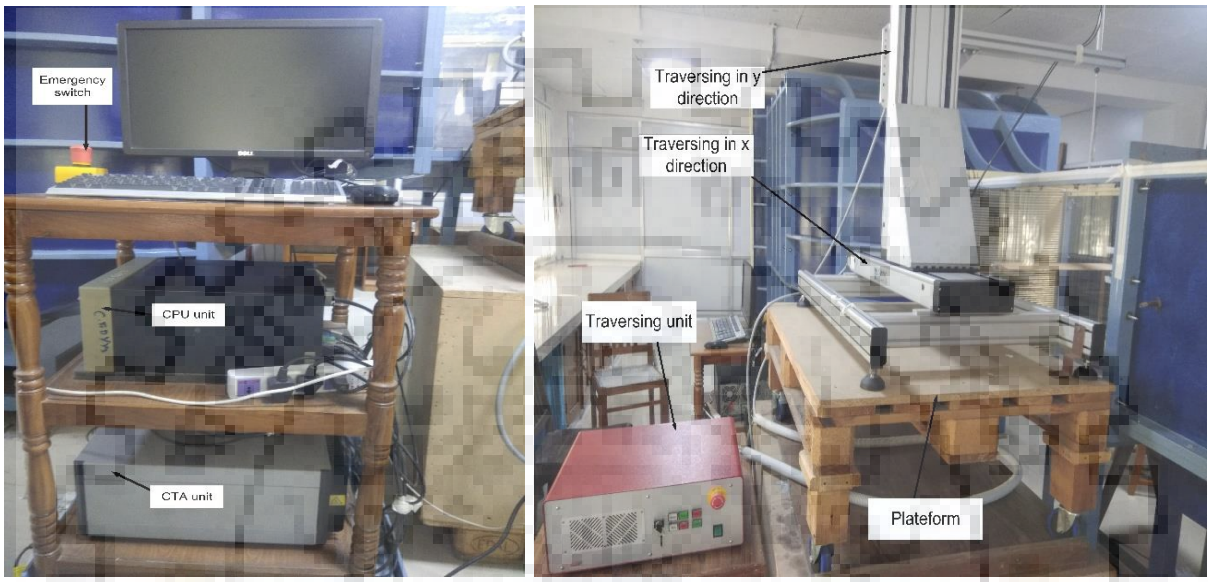

Fig. 4.1 Hotwire workstation (left), 2-D traversing system (right)

4.1 Hotwire anemometry

A two-channel hotwire anemometer (Dantec Company) has been used for measurement of the flow fluctuation, mean velocity profile and turbulence intensity of incoming flow with and without the presence of shear screen and airfoil as shown in figure 4.2.

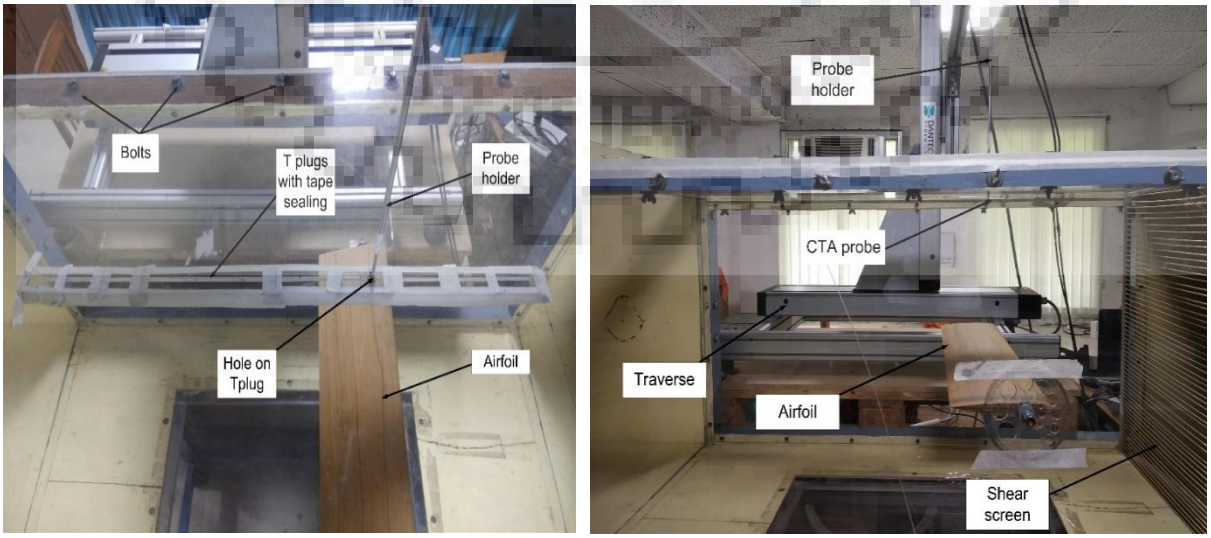

Fig. 4.2 Hotwire probe at the top position without (left) and with (right) a shear screen.

Working principle of hot wire anemometer is based on the principle of compensation of the rate of heat loss from a small heated metallic wire when it is exposed to the flow. When any change in the flow takes place then this leads to a change in heat transfer from the wire. Hence reducing the temperature of the wire. Since the resistance of a wire depends upon the temperature of hot wire, therefore, there is a change in the resistance of a wire. This change in resistance is monitored by a feedback circuit. This feedback circuit allows more current hence voltage to the circuit till wire temperature is maintained constant. This change in voltage is calibrated with the flow. With this process, it is possible to measure the fluid velocity accurately. This hot wire has a limitation that it is insensitive to the direction of flow.

To understand the basic principle of working of hotwire anemometer (constant temperature type) a schematic figure 4.3 shows a Wheatstone bridge having a resistance of R_1, R_2, R_3, and fourth resistance is the sensing wire which is having higher

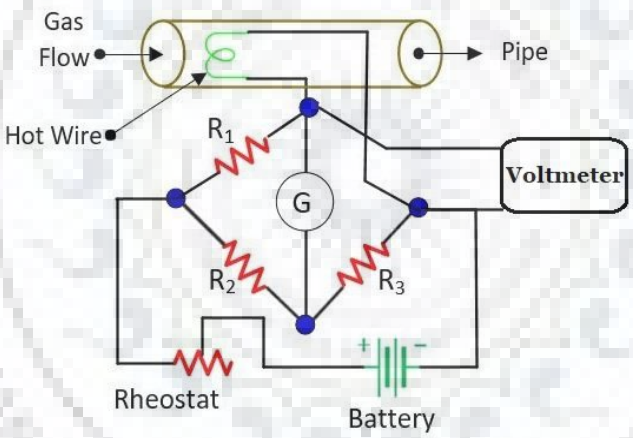

Fig. 4.3 Circuit diagram of constant temperature (CTA) from www.circuitglobe.com

Temperature (150-250ºC). When the flow starts then gas or air comes in contact with hot wire and heat is transferred to the air due to that temperature of wire decrease. Since at beginning by adjusting the rheostat galvanometer is set to zero but now due to change in the temperature of wire its resistance changes hence Wheatstone bridge becomes unbalanced. Hence to balance this, the current is allowed to move through bridge this current is calibrated with the flow of air. After balancing of Wheatstone bridge the voltage difference is calculated by voltmeter which is calibrated. In this way velocity of wind is measured through the hot wire anemometer. To determine time average velocity, velocity fluctuation or turbulence intensity since the probe cannot measure continuous data hence to measure discrete data it is necessary that the integral time scale of sampling must be at least two times larger than the integral time scale of velocity

fluctuation. In this way, all the physics associated with flow fluctuation can be captured with the probe. Single wire probe is set with the sampling frequency of 1 kHz for two seconds to measure the velocity above airfoil surface and to measure velocity profile for both with and without shear screen, in the far wake downstream side sample size of 20,000 with same sample frequency is set. The probe is placed at 0.5C from the trailing edge to get the vortex shedding frequency of uniform inflow and uniform shear flow.

4.2 Hotwire probe and probe support

Hotwire anemometer consists of a probe with the probe support cable, CTA, signal conditioner, analog to digital convertor and computer system. A Dantec model 55P11 single wire probe is used for taking the measurements. This probe consists one of 5 µm diameter and 1.25mm long wire, made up of platinum plated tungsten material.

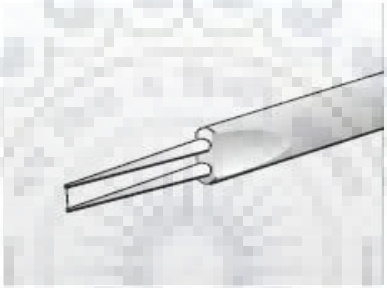

Fig. 4.4 Miniature of single wire probe www.dantecdynamics.com

Hotwire probe, A/D converter, CTA anemometer are connected to the computer system. The probe responds primarily velocity vector. The measured voltage is then allowed to pass through signal conditioning to filter the noise to improve the single strength. The normal operating temperature of the hot wire probe is 150-250ºC for flow measurements. In this experiment operating temperature of probe is set to 150ºC. This temperature is very important because this reduces the effect of radiation hence reduces the errors which are more significant in the low-velocity region as in the recirculation bubble. Higher temperature reduces the sensitivity of wire and also this also leads to oxidation of wire.

4.3 Data acquisition system

The output of the CTA is continuous data obtained is analogous voltage continues signals. These data are acquired and processed by the Stream Ware proV5.02 software. In order to process it digitally, it has to be sampled as a time series consisting of discrete values digitized by an analogue to digital converter (A/D board). A/D board is configured to avoid the noise present in a continuous signal and also amplified. The frequency of converting continuous data

into discrete data and number of samples depends upon the choice of A/D board. Hotwire signal is acquired through 12 bit A/D data acquisition card (DAQ) (Company-National instruments, model PCI-6251) and 68 pins SCB-68 termination I/O connector. The DAQ board has 2 analogue input channel and 2 analogue output channel

4.4 Pitot-static tube and micro-manometer

The Pitot - static tube is the instrument which is used to measure the velocity of flow. In this experiment pitot-static tube is used has L shape having a dimension of 70cm and 13cm in length, and outer diameter is 8mm as shown in figure 4.5. It has two pressure ports, one is for dynamic pressure and second for static pressure. It works on Bernoulli's principle. The pressure difference between static and dynamic points are measured by energy conversion velocity of the air is calculated.

Fig. 4.5 Pitot tube for calibration of velocity measured from hotwire anemometer.

Here the whole process of conversion is done by the Micro-Manometer. Two pressure port from the Pitot - static tube is connected to the high-quality differential pressure micro manometer (Furness Control company, model FC012) with pre-calibrated velocity output and a digital display as shown in figure 4.6. It is a capacitance type differential transducer it can measure pressure up to 1.99 mm of H_2O with a resolution of 0.01mm of H_2O.

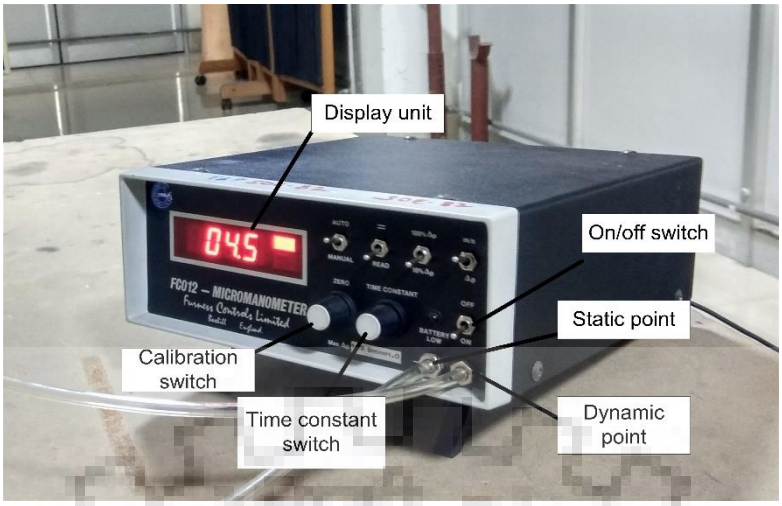

Fig. 4.6 Micro manometer for calibration of velocity measured from hotwire anemometer.

4.5 Calibration of hot wire

Calibration of hot wire is done by using a pitot-static tube connected to the micro manometer. For that, the probe and Pitot tube is placed at the centre point of the test section-2 but in a different plane at the time of calibration. The voltage acquired by the probe and the corresponding velocity is measured by the pitot-static tube.in this way, voltage and corresponding velocities are calibrated over a range of velocity. The software makes a relation between velocity and voltage from the data obtained from the Pitot - static tube and hot wire probe. A fifth order polynomial is fitted between velocity and voltage.

4.6 Data reduction

Data acquired by the probe is collected by the software as raw data. These signals are the voltage signals and are converted into velocity signals using calibration. Hotwire captures N number of samples at each location evenly, if the temporal velocity at a location is u in the x-direction and magnitude velocity component, here we call it free stream velocity is U and fluctuating velocity is $u'(t)$, since in our case single wire probe is used which capture x-direction velocity fluctuation only, then

$$U_x = \frac{1}{N}\sum_{i=1}^{N} u_i$$

$$U = \sqrt{{U_x}^2 + {U_y}^2 + {U_z}^2}$$

$$u'(t) = u(t) - U$$

and the root mean square value of the local or temporal velocity (u_x') in x-direction

$$u_x' = \sqrt{\frac{1}{N}\sum_{i=1}^{N} u'(t)^2}$$

4.7 Drag coefficient (C_D) by wake survey method:

To obtain the drag coefficient principle of linear momentum is used. This method is discussed in Schlichting (1979). This method required two velocity profile one profile of free stream and second at the location where static pressure does not vary across the direction of flow. At this location, the profile has a wake zone. In these two zones, linear momentum conservation is the direction of flow is applied. The formula for Cd is given below

$$c_D = 2\int_{-\infty}^{\infty} \frac{u}{U}\left(1-\frac{u}{U}\right)dy$$

Where,

u is the local velocity and U is the free stream velocity. For uniform shear inflow case, U is the free stream velocity upstream side of the shear screen for chord-based Reynolds number of 4×10^4 and 8×10^4.

4.8 Design of shear screen

The design of the shear screen is adapted from Owen P.R. and Zienkiewicz H.K. 1957 the design is based on the principle that by providing resistance to the flow gradient in the velocity across the direction of flow can be obtained. To provide resistance to the flow, here number of circular rods are used. The important point for design is that after placing rods the static pressure before and after the rod in the direction of flow should not change, but total pressure will definitely change. The change is static pressure upstream and downstream side of the flow will cause the introduction of ω_x, ω_y. Constant total pressure difference leads to a constant value of ω_z. On the basis of the design principle, 58 rods having a dimension of 60cm length and 3mm diameter is used and made up copper. Higher diameter rod may lead to the introduction of x and y vortices, which will disturb the shear effect. Each rod is having 1.5 mm diameter hole on both sides of the cross-section.

Fig. 4.7 Image of a copper rod used for screen

These rods (fig. 4.7) are screwed on the aluminium frame having a length of 60cm.wigth of 1.5cm and thickness of 3mm. minimum thickness of strip was required because it will resist the flow and also may introduceω_y.To screw the rods on the strip, similar holes are prepared on the strip. The location of holes hence rods are according to the design of the screen. The design formula used for shear screen is given below

$$\frac{\xi}{\left(1-\xi^2\right)} = k_0\left[1-2\frac{\lambda h}{U}\left(\frac{1}{k_0}+\frac{1}{1+a}\right)\left(\frac{y}{h}-\frac{1}{2}\right)\right]$$

$\xi = {}^{d}/_{s}$ where d and s are diameter and spacing between the rods respectively. The value of k_0 is the resistance coefficient which value is taken 1.15. λ is a shear gradient, h is the height of screen U is the upstream velocity far from the screen. Constant values $\frac{\lambda h}{U}$ and a are taken from Owen P.R. and Zienkiewicz H.K. 1957.

Based on this relation graph platted shown below-

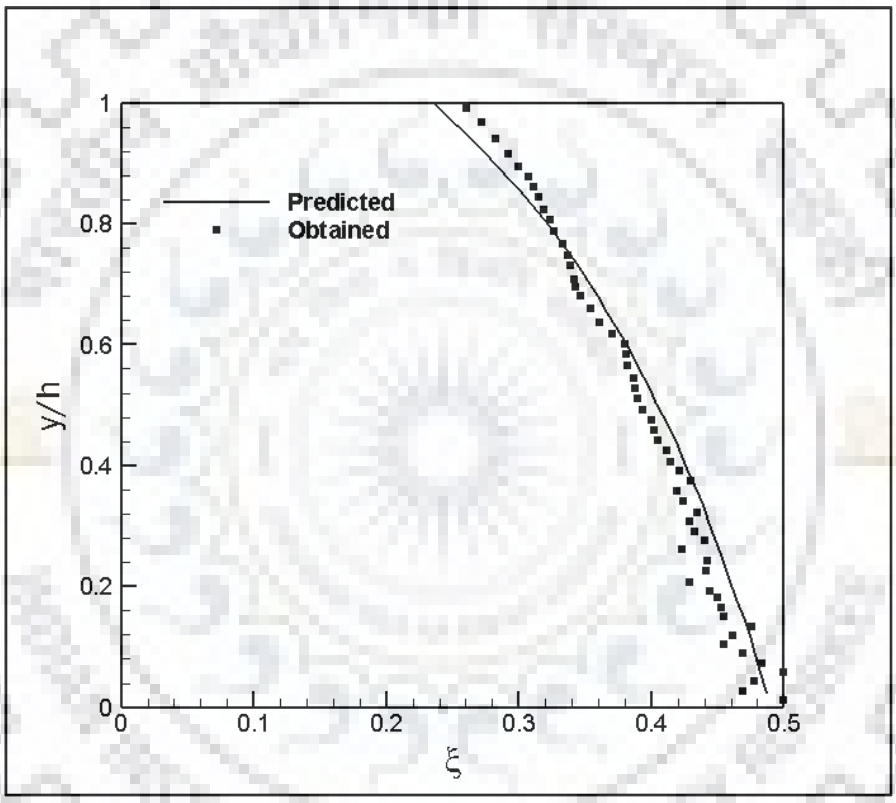

Fig. 4.8 Graph of the spacing and location of the rod (predicted and obtained)

Since Aluminium strips are very thin for giving rigidity to the screen, over tightening of any rod leads to buckling of neighbouring rod hence we had to compromise with the rigidity of screen for maintaining straightness of rod. Due to the self-weight of the rod sagging in the rod takes place which is also mentioned in previous literature. At a few locations due to loosing of rod vibration took place at Re=8×10^4. After fabrication of rods with strip, the screen is placed. The shear screen is not much rigid but due to the close fitting of the screen in the test section, there is no deformation in the screen was noticed at any Reynolds number.

Fig. 4.9 Image of the shear screen (front view)

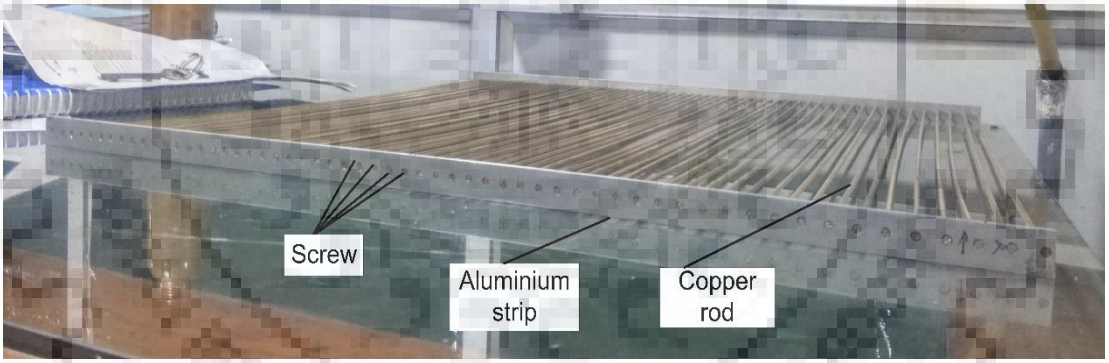

Fig. 4.10 Image of the shear screen (Side view)

To insert the screen inside the test section the top acrylic sheet was removed and the screen was placed and then the acrylic sheet was bolted. To remove the screen the same procedure was followed.

4.9 Procedure to measure the velocity above the airfoil surface

To do the comparison between shear flow and uniform flow above the airfoil surface CTA probe is placed above the airfoil which moves from 3mm above the airfoil surface to 4 cm below the top sheet. To capture the flow just above the airfoil the probe is placed at 6 different location varying from 0.5cm, 3cm, 6cm, 9cm, 12cm and 15cm from the leading edge in the direction of flow. The probe could not be placed at just leading edge because the probe is fixed in probe holder having "L" shape. Readings through CTA probe were taken for both cases when inflow was sheared and when inflow was uniform for all five angles of attack of airfoil varying from 0°,3°,6°,9° and 12°. The effect of shear flow with the uniform flow over the airfoil surface.

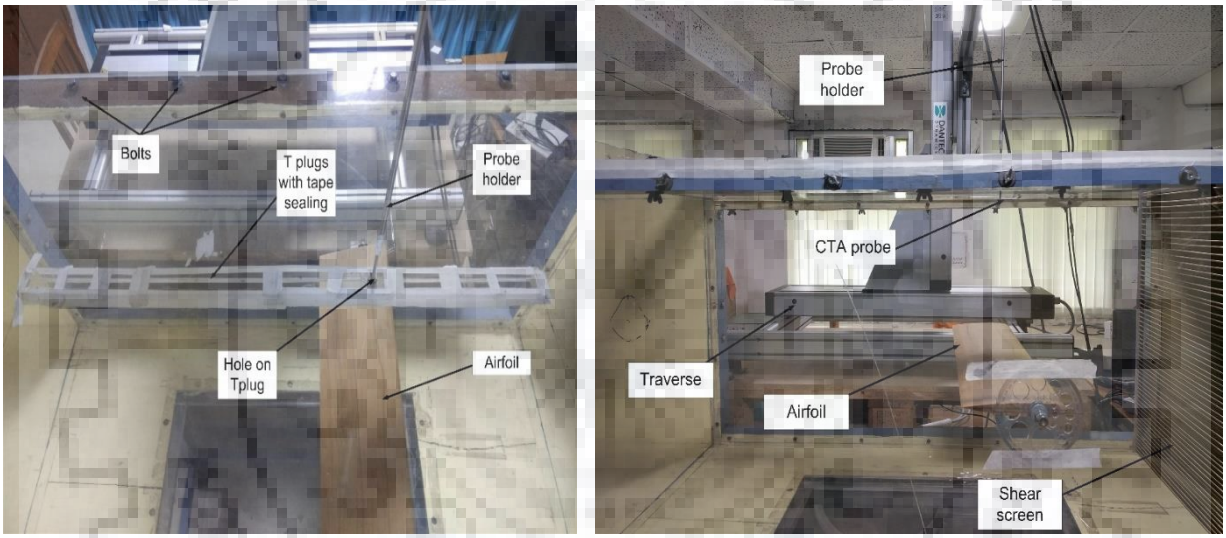

Fig. 4.11 Hotwire probe at the top position without (left) and with shear screen (right)

4.10 Procedure to measure the mean velocity profile

To do the comparison of time average velocity profile of shear flow and uniform flow past an airfoil, readings were taken from Pitot - static tube and hot wire.

Manual traverse is used to hold and to give the vertical movement to the Pitot - static tube. With this pitot-static tube velocity readings were taken at three different location $^{x}/_{c} =$ 9,12,15 in the direction of flow, with and without the shear screen at a different angle of attacks 0°,3°,6°,9° and 12°. Traverse is moved manually from one location to another location and to give the vertical motion to the Pitot - static tube, rotating mechanism is used available in the traverse.

While taking the velocity readings CTA probe was placed at the location $^{x}/_{c} = 10$. To cover the whole height of the test section a total of 250 points are taken in the interval of 2 mm. CTA probe captures 20,000 samples in every 2 seconds.

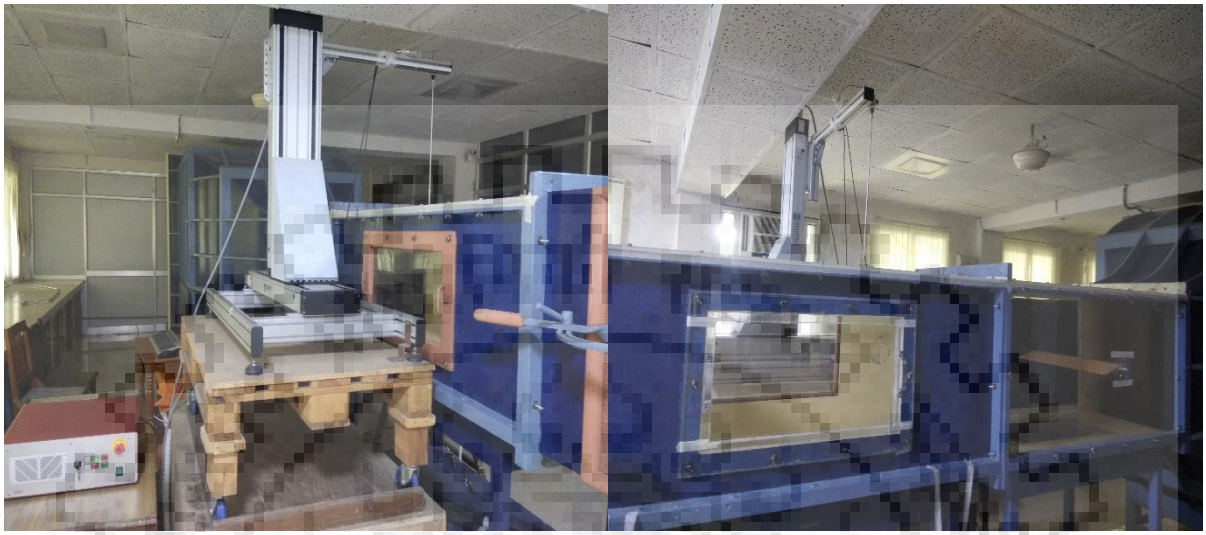

Fig. 4.12 Image of traverse unit while taking readings in test section 2

Chapter 5 Result and discussion

The experiments for uniform inflow and uniform shear flow over an airfoil NACA 0012. The flow is characterized by a hot wire anemometer setup. NACA co-ordinate 0012 is selected because a number of experiments have been done with this airfoil hence the availability of data for validation purpose. Experiments have been done with a sample rate of 1 kHz for 2 seconds when the CTA probe was allowed to move from airfoil surface to near the test section surface in transverse direction probe was not allowed to reach more than 3 mm for the safety of CTA probe. While doing the experiment to get the mean velocity profile with and without profile for both the inflow condition sample size of 2000 at 1 kHz sampling rate was not adequate to capture the flow fluctuation in the far wake hence the sample size of 20000 was chosen for the same sampling frequency. The experiments were taken during such a span of time when there is not much variation in the temperature of the environment.

5.1 Flow quality in the test section

The flow in the working test section is found to be uniform when the shear screen is not placed inside the test section. Two velocities 4.6 and 7.7 are selected for the experiment. Whereas when the shear screen is placed inside the test section 1 and velocity reading were taken by CTA anemometer, then a uniform gradient is in the inflow is obtained for respective Reynolds number which follows the velocity equation

$$u_1(y) = 4.6 + \lambda_1 \left(y - \frac{h}{2}\right)$$

$$u_2(y) = 7.7 + \lambda_2 \left(y - \frac{h}{2}\right)$$

Where, the first and second equation indicates the velocities for Re of 4×10^4 and 8×10^4 respectively. The value of $\lambda_1$and λ_1 are 0.495 and 0.833. The shear parameter (K) remains constant for both Reynolds number which is 0.0161, this indicates a weak shear. The two uniform profiles, as well as the shear profiles are found to be stable in nature

5.2 Turbulence intensity of flow

The turbulence intensity of incoming uniform free stream is measured with Hotwire Anemometer shown in the given table below

Reynolds number	Uniform inflow (TI)	Uniform shear flow (TI)
4×10^4	0.0029%	0.00945%
8×10^4	0.00228%	0.0076%

Table no. 5.1 Table for turbulence intensity (TI)

When the shear screen is placed inside the test section then mean velocity profiles for both Reynolds number, measured with hot wire anemometer are shown in the figure 5.1 Image of the both the velocity profile of uniform inflow and uniform shear flow ($Re_{freestream}=4\times10^4$).

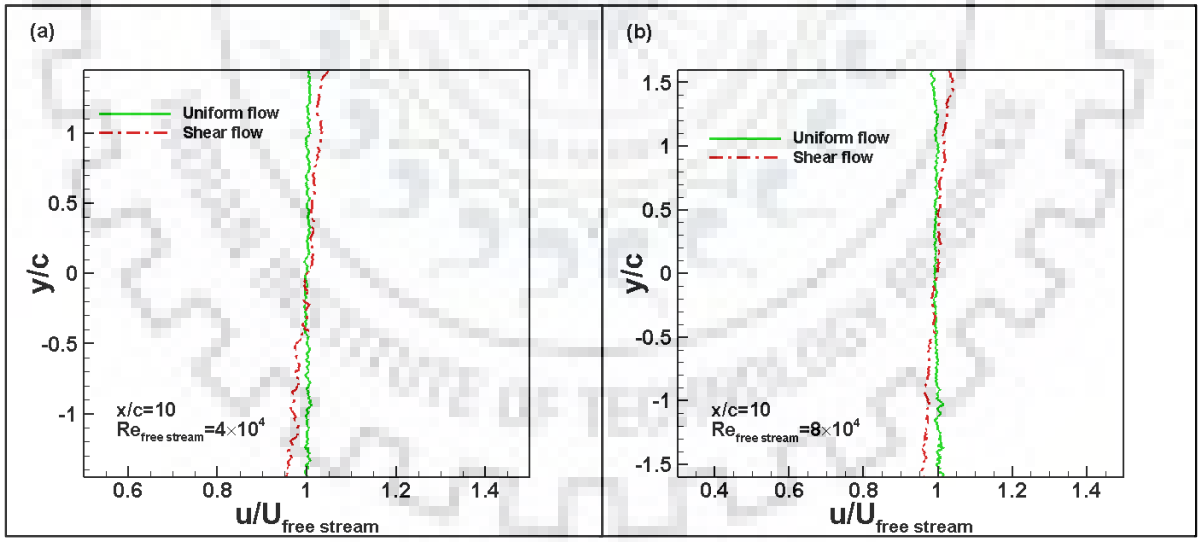

Fig. 5.1 Profile of velocity magnitude for uniform inflow and shear inflow.

5.3 Velocity profile far wake from airfoil with both configurations (Hotwire manometer)

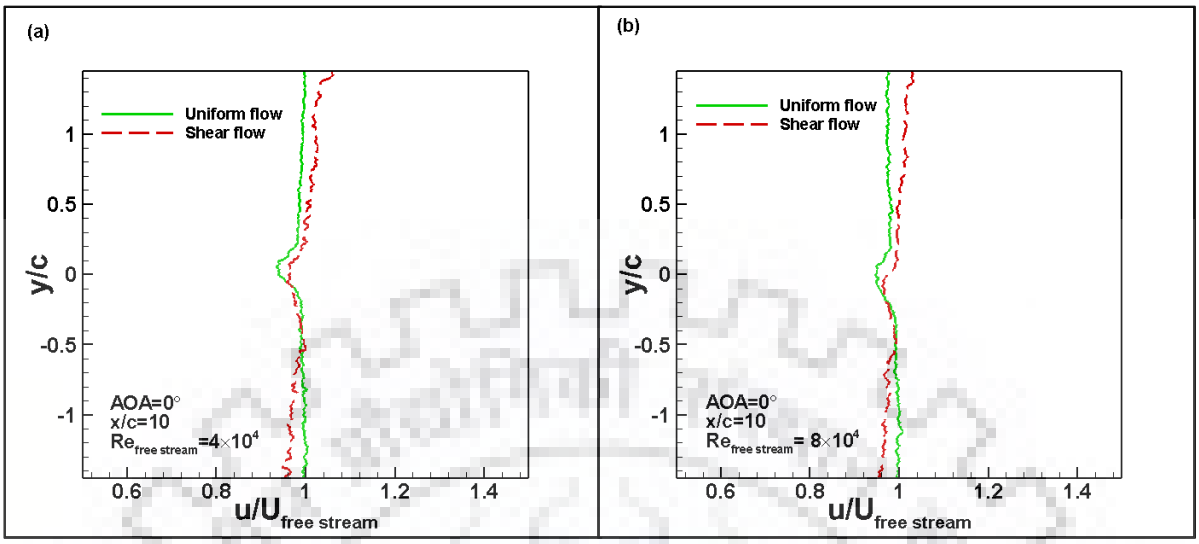

Fig. 5.2 Velocity magnitude plots of two configurations (0º angles of attack).

Figure5.2 represents the far wake velocity profile for both inflow conditions for 0º angles of attack. In the figure 5.2(a) the lower Reynolds number regimes and figure 5.2(b) represents higher Reynolds number regimes. Both the figure shows shifting of the wake zone vertically of shear inflow, compared to that of uniform inflow also velocity deficit reduces. Compare to the wake zone of uniform inflow, the wake zone of uniform shear flow is smaller marginally. This is possible because of higher momentum in the boundary layer on the suction side which can be seen in the velocity profile diagram above the airfoil surface figure 5.8

Figure 5.3 represents the far wake velocity profile for both inflow conditions for 3º angles of attack. A small fluctuation in velocity magnitude is observed in the lower Reynolds number regimes for shear flow. Here also the same vertical wake zone shifting is observed but it is higher for lower Reynolds number. A very small velocity deficit is noticed for both the cases. The decrement in wake width is higher for lower Reynolds number compare to higher Reynolds number.

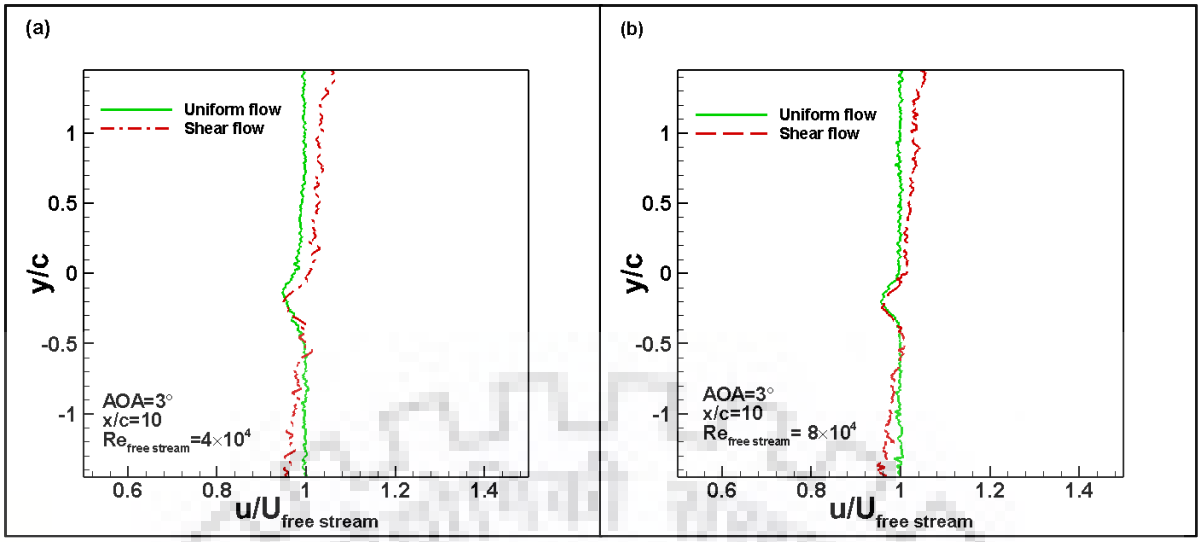

Fig. 5.3 Velocity magnitude plot of two configurations (3º angle of attack).

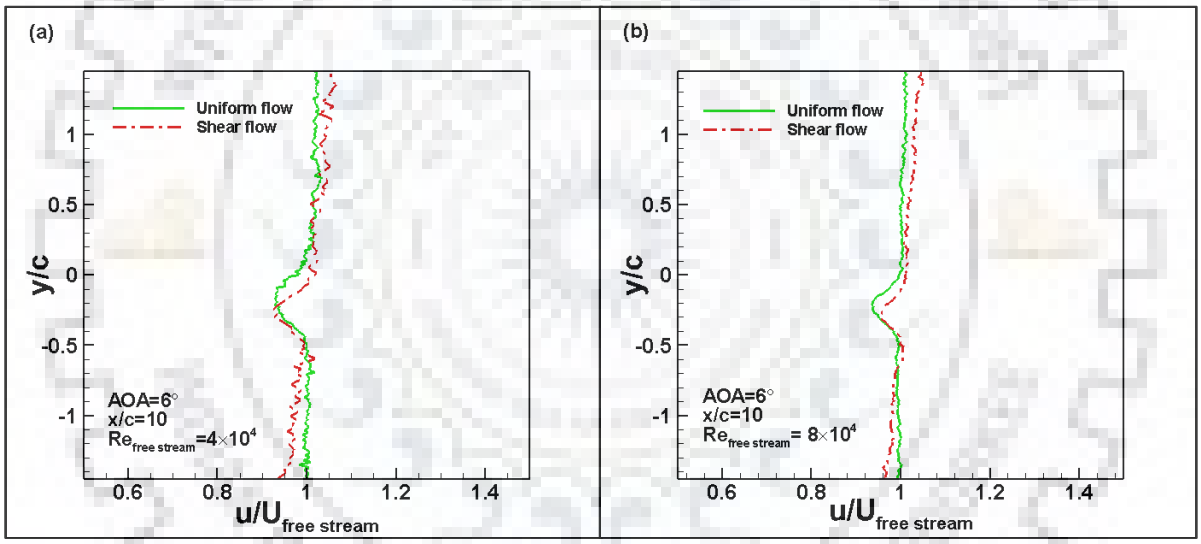

Fig. 5.4 Velocity magnitude plot of two configurations (6º angle of attack).

Figure 5.4 represents the far wake velocity profile for both inflow conditions for 6º angles of attack. More fluctuation in velocity magnitude is observed than the previous case of the lower Reynolds number regimes for shear flow. For both cases, wake zone shifts vertically. Velocity deficit takes place for shear flow in high Reynolds number regime but negligible velocity deficit is observed for low Reynolds number regimes.

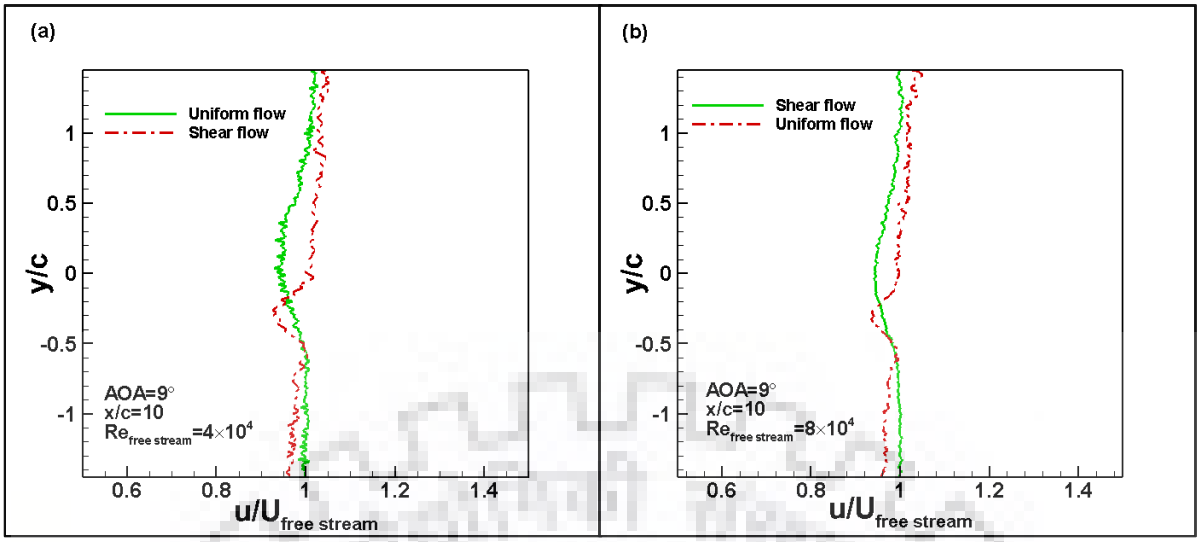

Fig. 5.5 Velocity magnitude plot of two configurations (9º angle of attack).

Figure 5.5 represents the far wake velocity profile for both inflow conditions for 9º angles of attack. The significant effect of shear inflow is observed in this angle of attack for both Reynolds number regimes. The major vertical shift of the wake zone is observed for both flow regimes. Wake zone decreases significantly for both flow regime. Although the velocity deficit increases marginally.

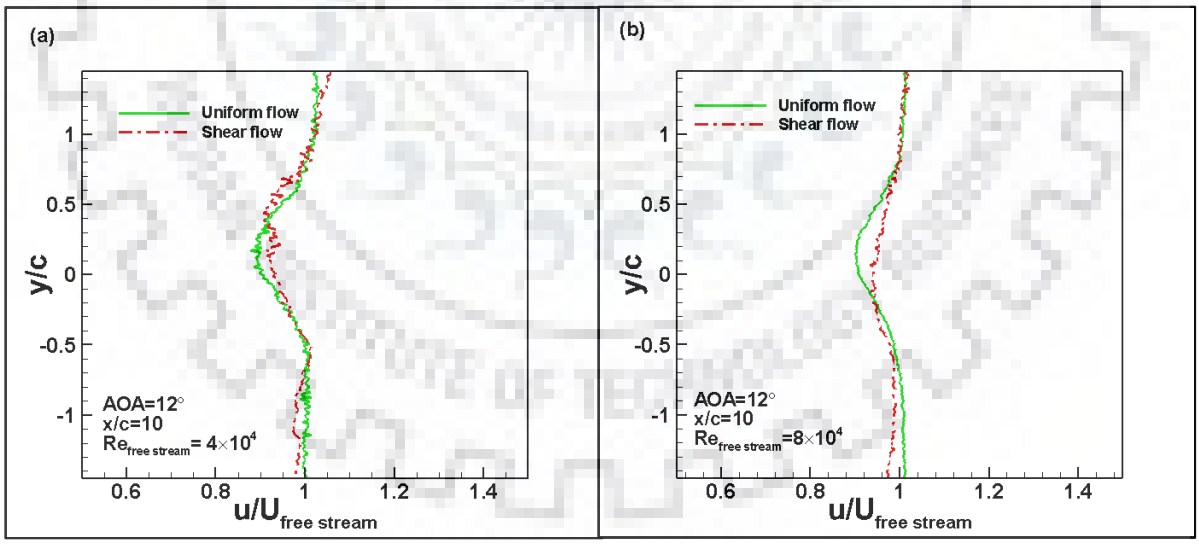

Fig. 5.6 Velocity magnitude plot of two configurations (12º angle of attack).

Figure 5.6 represents the far wake velocity profile for both inflow conditions for 12º angles of attack. There is no significant difference in the size of the wake zone for both the Reynolds number. Unlike to other Reynolds number here wake, zone shift upward in low Reynolds number regime but for higher Reynolds number flow regime, it moves downward.

Higher velocity deficit was recorded for higher Re regimes as compare to lower Re flow regimes.

5.4 Velocity magnitudes profile over suction surface of airfoil

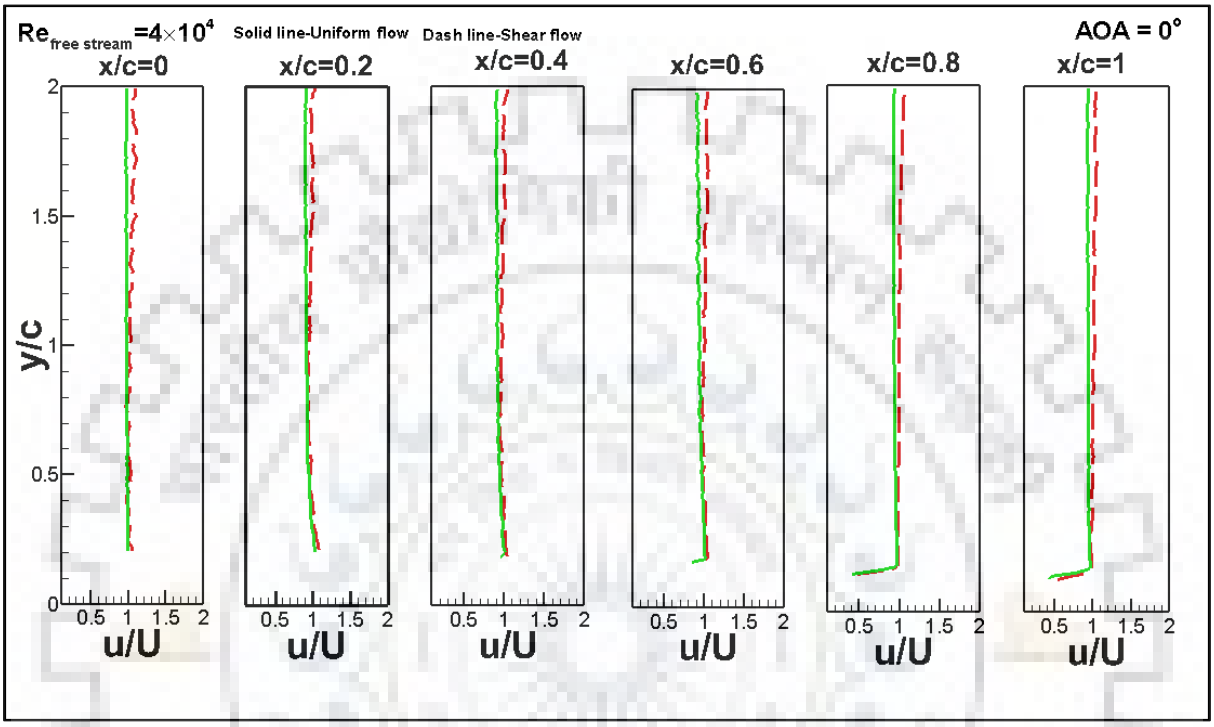

Fig. 5.7 Velocity profile over airfoil surface at 0º angle of attack in $Re_{freestream}$ =4×10^4.

Fig 5.7 represents the velocity profile for 0º angle of attack over the airfoil surface. The almost same path is followed by the velocity profile at zero angle of attack and low Reynolds number the velocity profile for uniform free stream inflow and shear inflow are almost identical at all different downstream location over the suction surface of the airfoil.

Whereas at high Reynolds number the difference in the velocity profiles figure5.8 of the uniform free stream and uniform shear flow is found at x/c=0.8 and x/c=1 downstream location where a certain drop in velocity is found near the suction surface in the uniform free stream flow case. This shows that the boundary layer separation is sifted downstream in the case of uniform shear inflow.

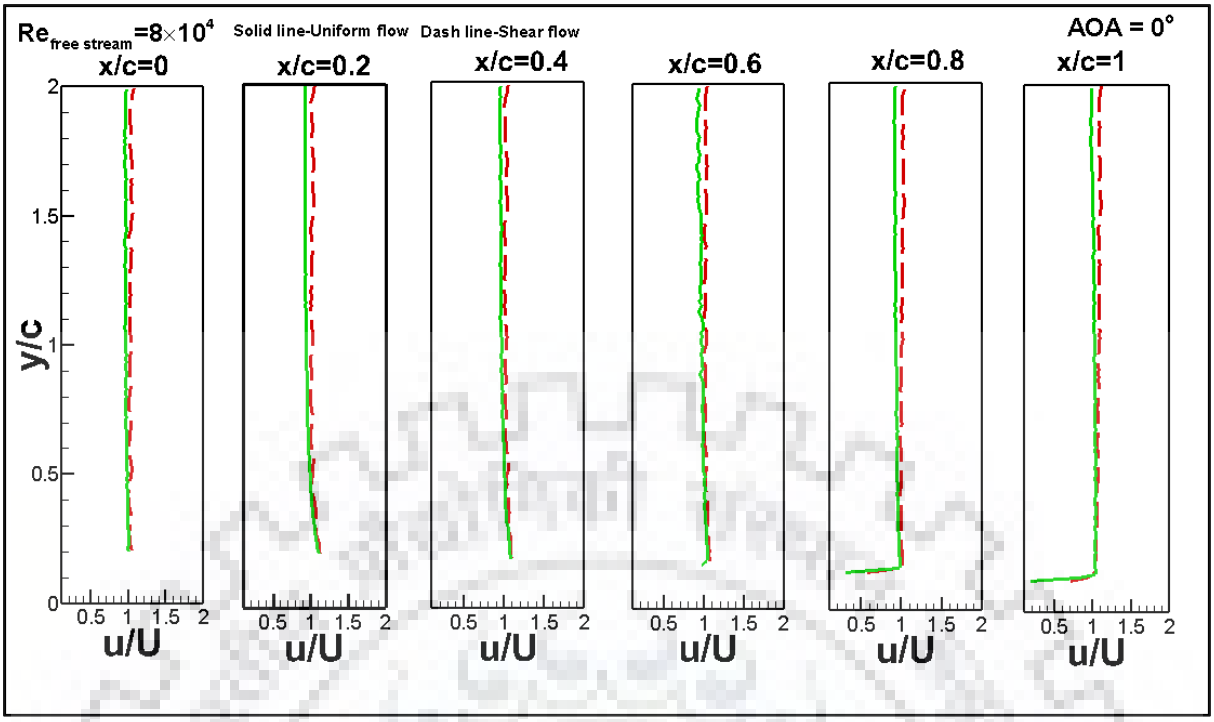

Fig. 5.8 Velocity profile over airfoil surface at 0º angle of attack in $Re_{freestream}$ =8×10^4.

Similar to the result of 0º angle of attack at low Reynolds number and 3º angle of attack, the effect of shear inflow seems to be missing as both velocity profile for the both of the cases are identical. The similar wake structure as shown in figure 5.2 has already been discussed.

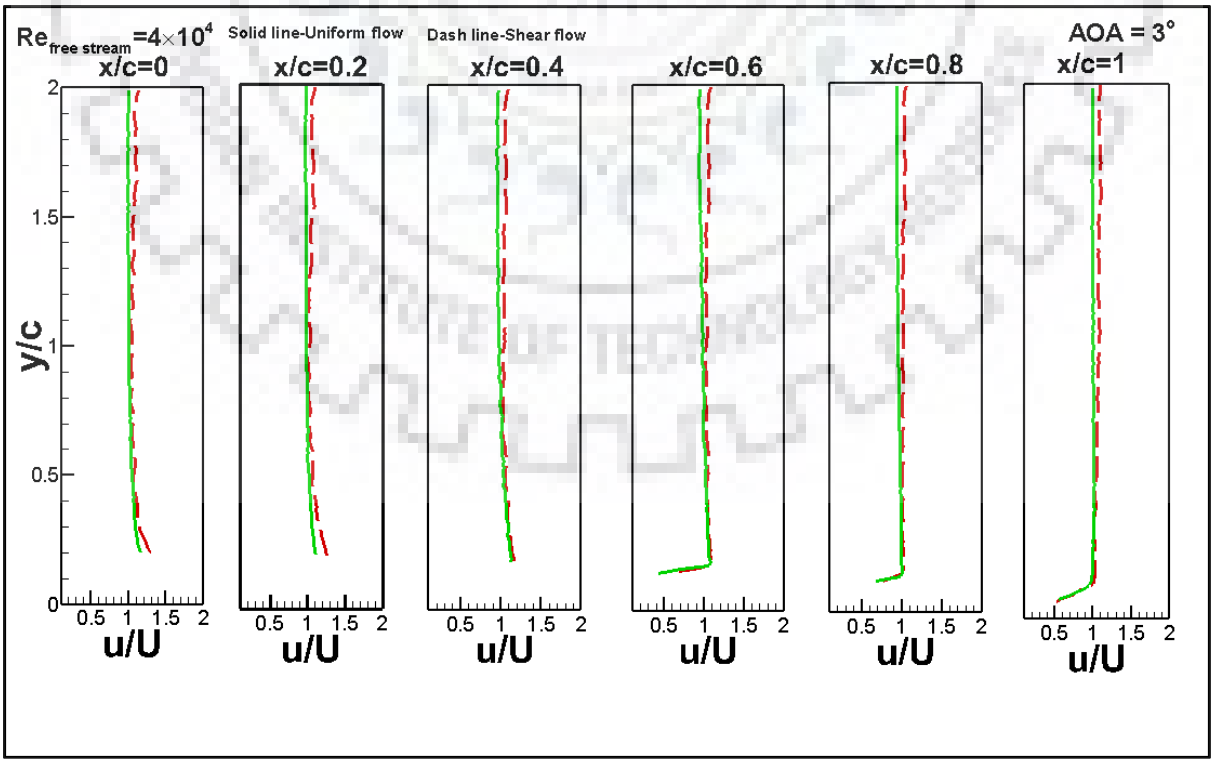

Fig. 5.9 Velocity profile over airfoil over airfoil at 3º angle of attack in $Re_{freestream}$ =4×10^4.

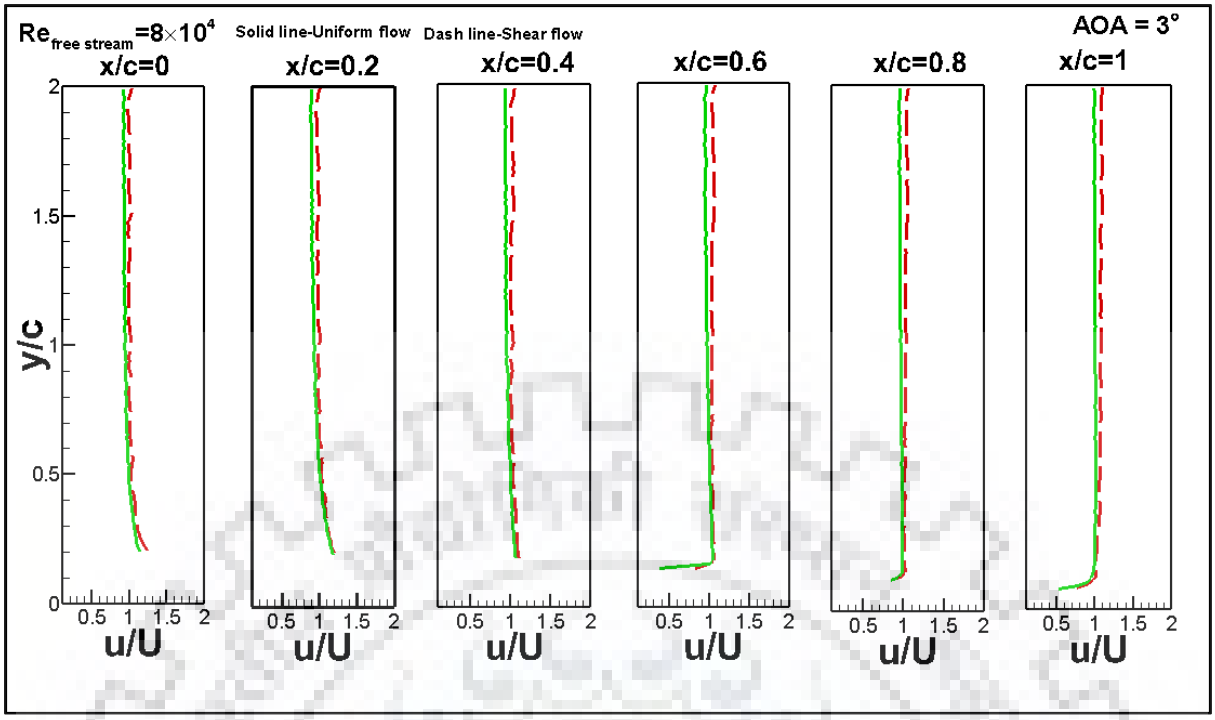

Fig. 5.10 Velocity profile over airfoil surface at 3º angle of attack in $Re_{freestream}$ =8×10^4.

From the platted velocity diagram it can be seen that difference in the velocity profile of the free stream and uniform shear flow (figure 5.10) is found at x/c= 0.6 and x/c=1 downstream location, where the drop in velocity is found near the suction surface in the uniform free stream

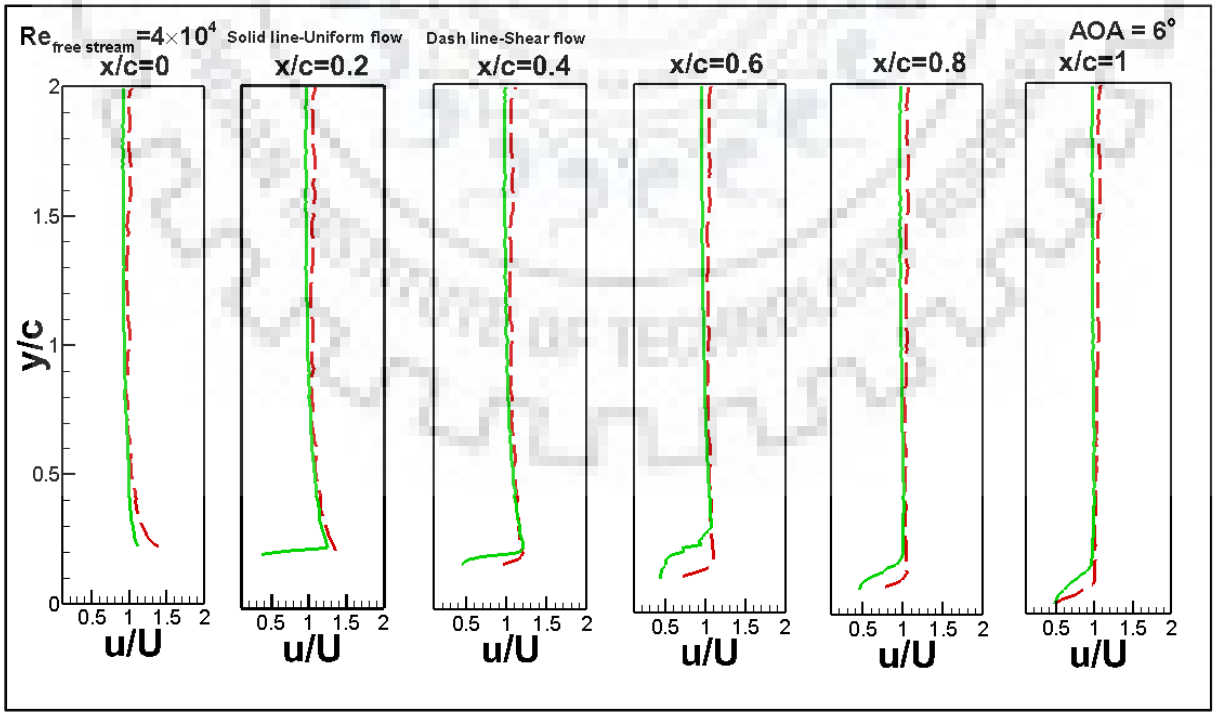

Fig. 5.11 Velocity profile over airfoil surface at 6º angle of attack in $Re_{freestream}$ =4×10^4

flow case. This shown the shear inflow has a higher tendency to resist the retardation of flow due to the adverse pressure gradient..

Figure 5.11 shows the velocity profile of uniform inflow and uniform shear inflow at an angle of attack of 6º over the suction surface of the airfoil. From a velocity profile, it can see that the significant velocity drop takes place in uniform flow near the airfoil surface which is started from x/c=0.2 to 1. Whereas in shear flow due to higher turbulence velocity drop is lower.

For higher Reynolds number with the same configuration figure 5.12, it is observed that due to higher momentum, both the flow is capable to counter the retardation in the flow near the surface of the airfoil. Hence similar velocity profile is obtained. This is also reflected in figure 5.4. Far wake velocity profile of 6º angle of attack where the wake zone is bigger and more vertical shifting of wake in low Reynolds number flow regime.

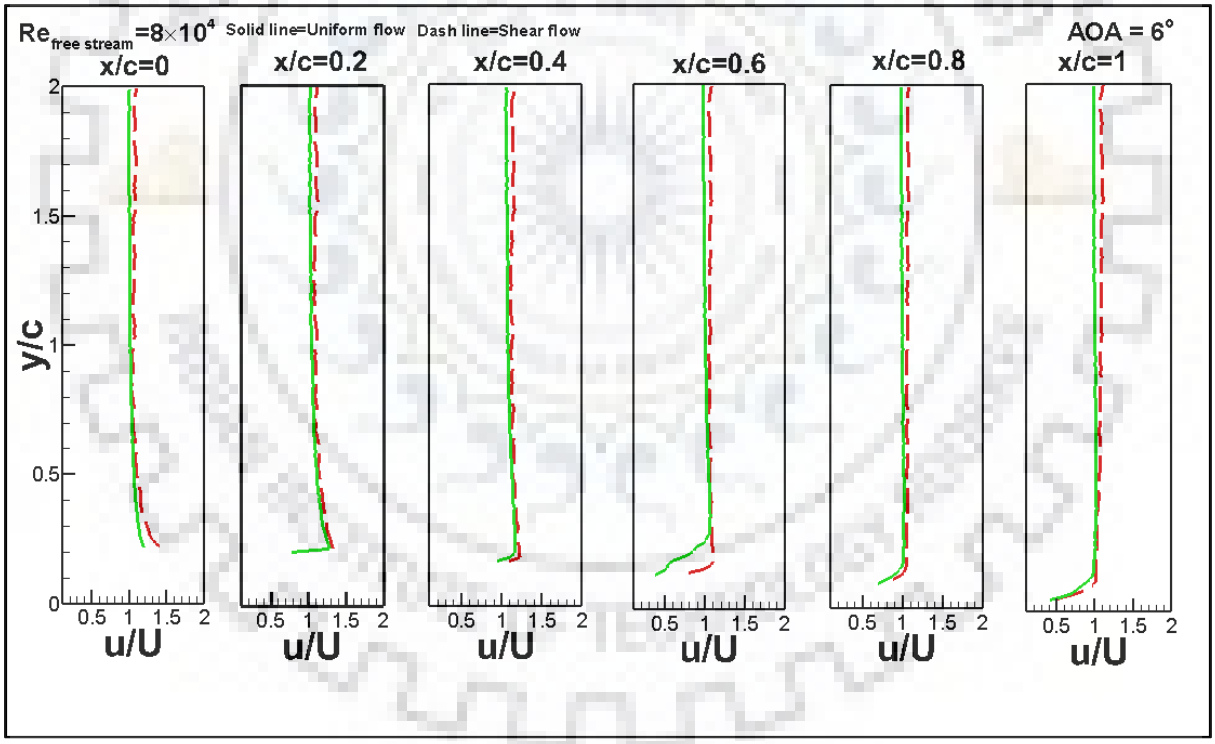

Fig. 5.12 Velocity profile over airfoil surface at 6 º angle of attack in $Re_{freestream}$ =8×10^4.

From the figure 5.13, it can be seen that in the angle of attack of 9º for both the Reynolds number of uniform inflow, the velocity retardation starts after x/c=0.2 which is due to the adverse pressure gradient and since uniform inflow has not much turbulence nature it is not

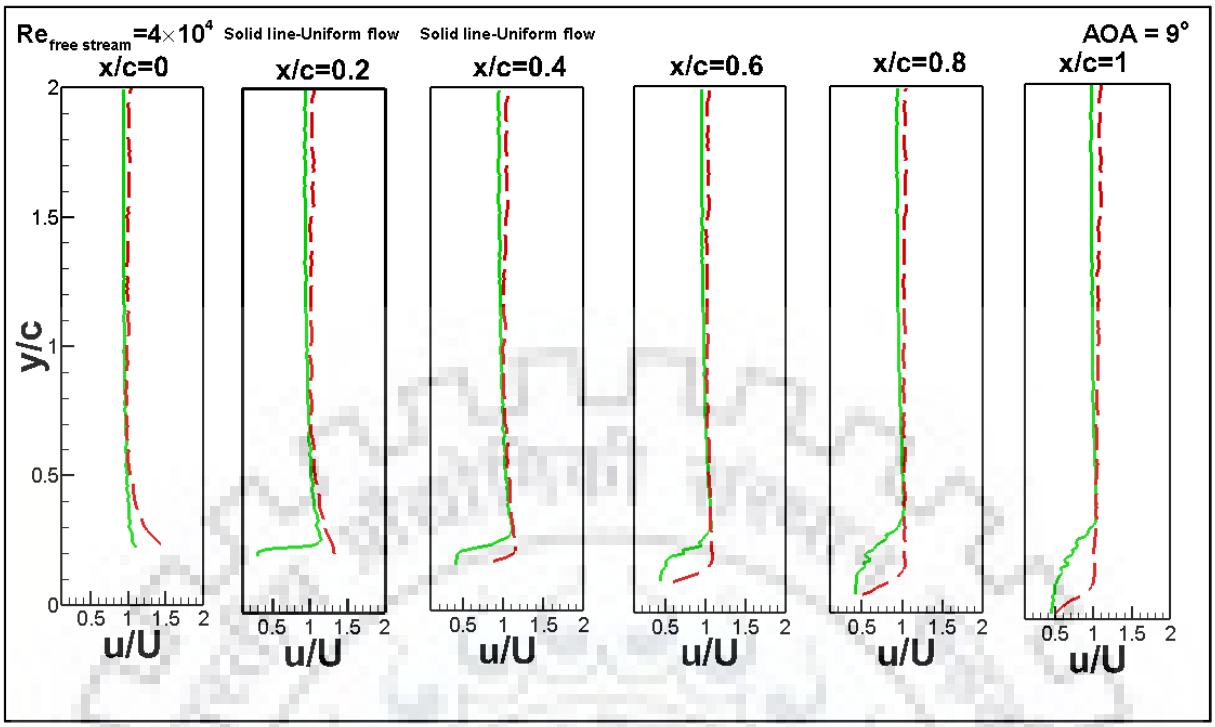

Fig. 5.13 Velocity profile over airfoil surface at 9º angle of attack in $Re_{freestream}$ =4×10^4.

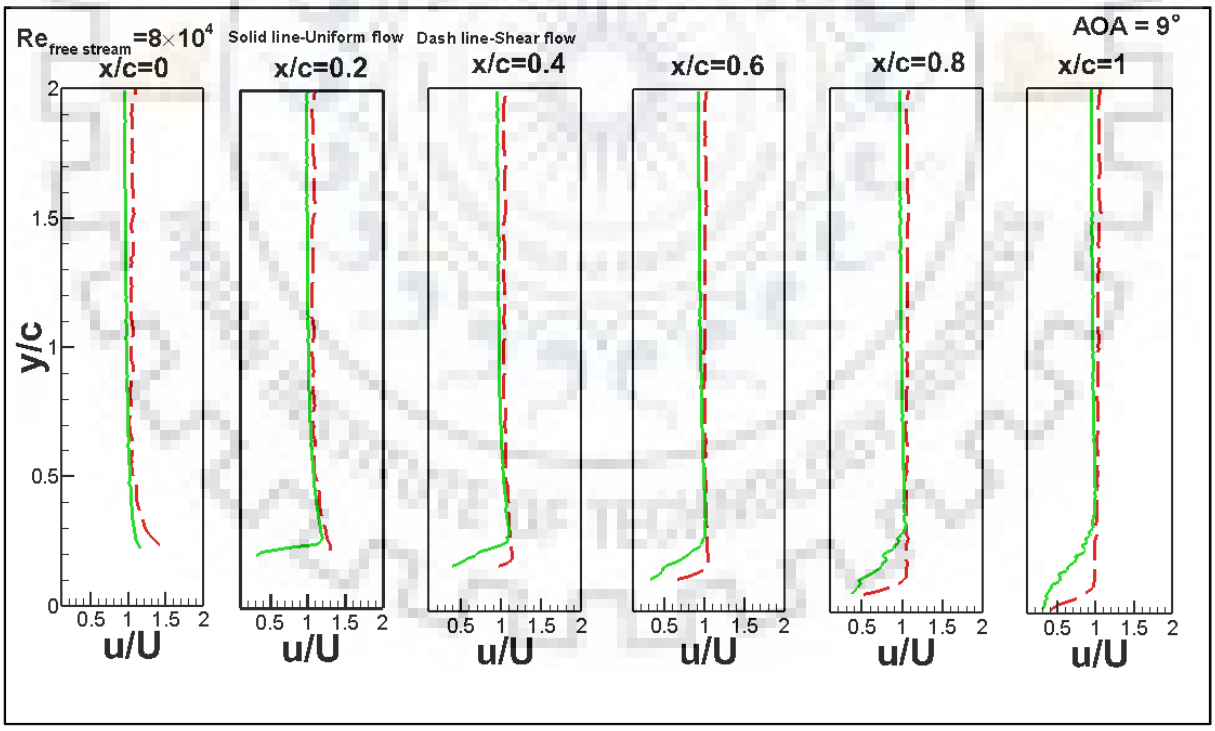

Fig. 5.14 Velocity profile over airfoil surface at 9º angle of attack in $Re_{freestream}$ =8×10^4.

capable to resist this drag hence sudden velocity drop takes place. Shear inflow has greater turbulence nature hence has a higher resistance to the adverse pressure gradient hence no sudden velocity drop takes place. This higher turbulence nature also lead to delay the flow

separation when pressure drag dominates, and due to delay in flow separation the wake zone reduces which can be seen in the figure 5.5 where the difference in the wake zone is significantly high and other difference of shear inflow profile from uniform inflow profile has been already discussed in the previous section.

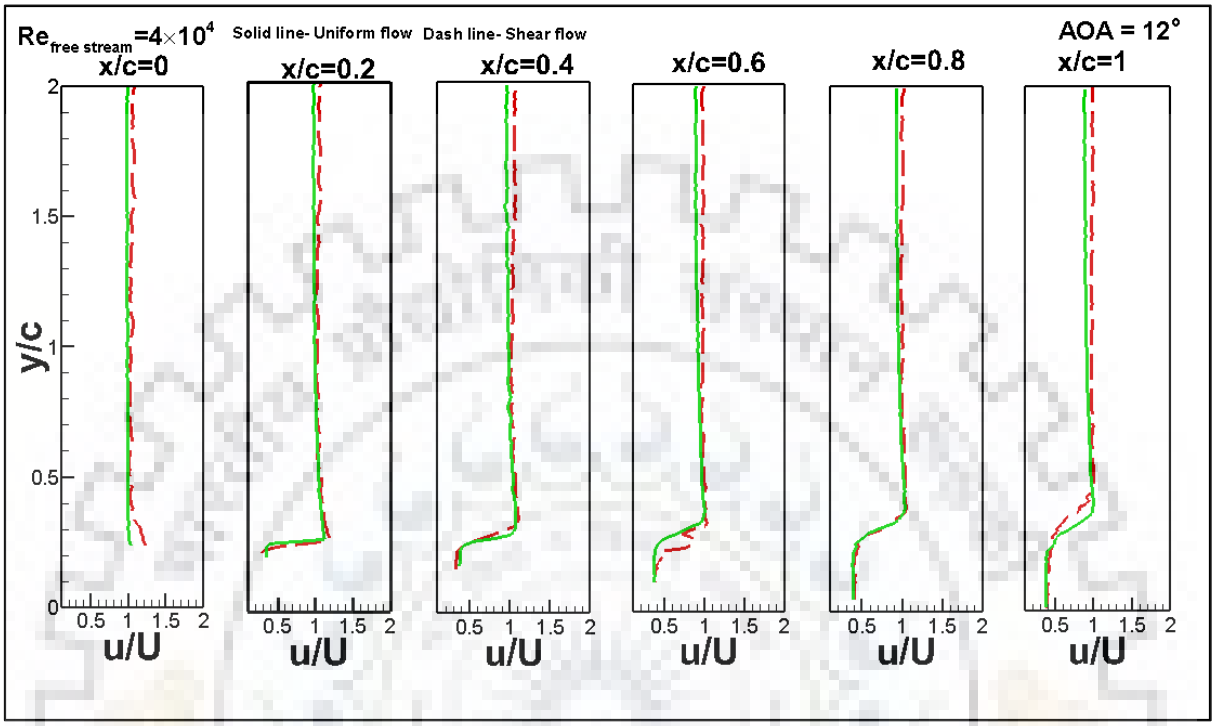

Fig. 5.15 Velocity profile over airfoil surface at 12º angle of attack in $Re_{freestream}$ =4×10^4.

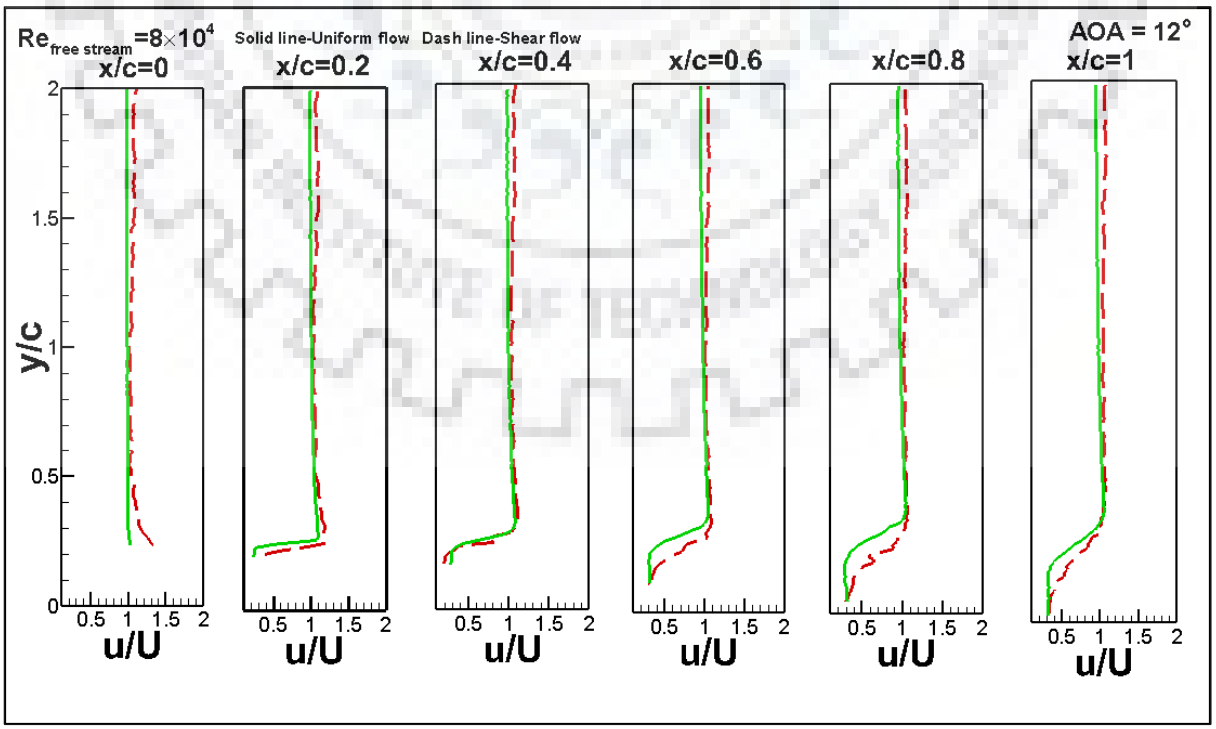

Fig. 5.16 Velocity profile over airfoil surface at 12º angle of attack in $Re_{freestream}$ =8×10^4.

Unlike the flow over airfoil at an angle of 9º, in 12º the pressure drag is much more dominating hence even higher turbulence present in the shear flow, but not much difference in flow profile is observed. Though the effect of turbulence in shear inflow is still noticeable in the flow regime especially for high Reynolds number.

5.5 Drag coefficient comparison:

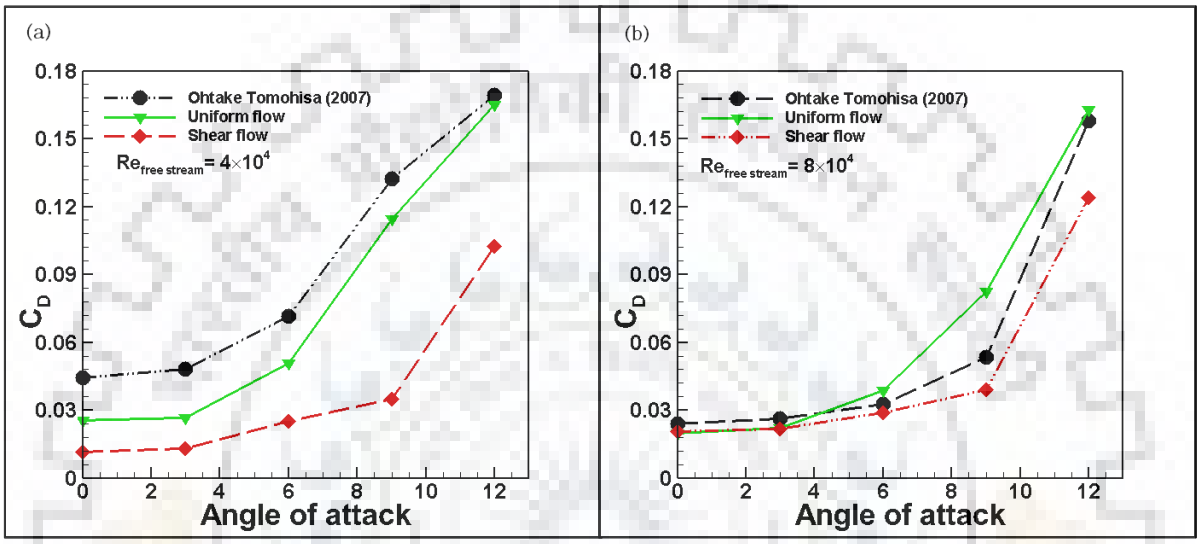

Fig.5.17 Platting of C_D with validation and comparison.

Figure 5.17 presents the mean drag coefficient obtained from the momentum balance between the upstream velocity and velocity profile at x/c = 10, downstream to the airfoil for both inflow conditions. Fig 5.17 (a) shows the drag coefficient for the uniform free stream condition for all AOA considered in the study for Re = 40,000. The C_D varies marginally up to AOA = 3º, then considerable increase is noticed up to 6º AOA. After that a steep increase in the Cd value is observed for 9º and 12º. The reason behind such trend is shifting of boundary layer separation upstream towards the leading edge of the airfoil with the increase of the AOA thus increasing low velocity region downstream of the airfoil. The steep drag at high AOA is due to onset of vortex shedding phenomenon in the wake of the cylinder thus behaving as a bluff body. In the figure 5.17 (a) also shows the trend of coefficient of drag for uniform shear inflow case for different AOA case. Lower C_D can be noticed in the figure for uniform shear inflow case with respect to uniform free stream inflow case, the reason being the delay in the shear layer separation off the suction surface for uniform shear inflow case. The sudden hike in at 12º AOA for uniform shear inflow case is due to onset of vortex shedding. Figure 5.17 (b) shows the C_D trend for uniform free stream inflow and uniform shear inflow case at Re =

80,000. The trends are similar to Re = 40,000 case. The results are in well accordance with the similar literature work (mentioned in the figures).

5.6 Velocity profile in the far wake from airfoil (measured with Hotwire anemometer)

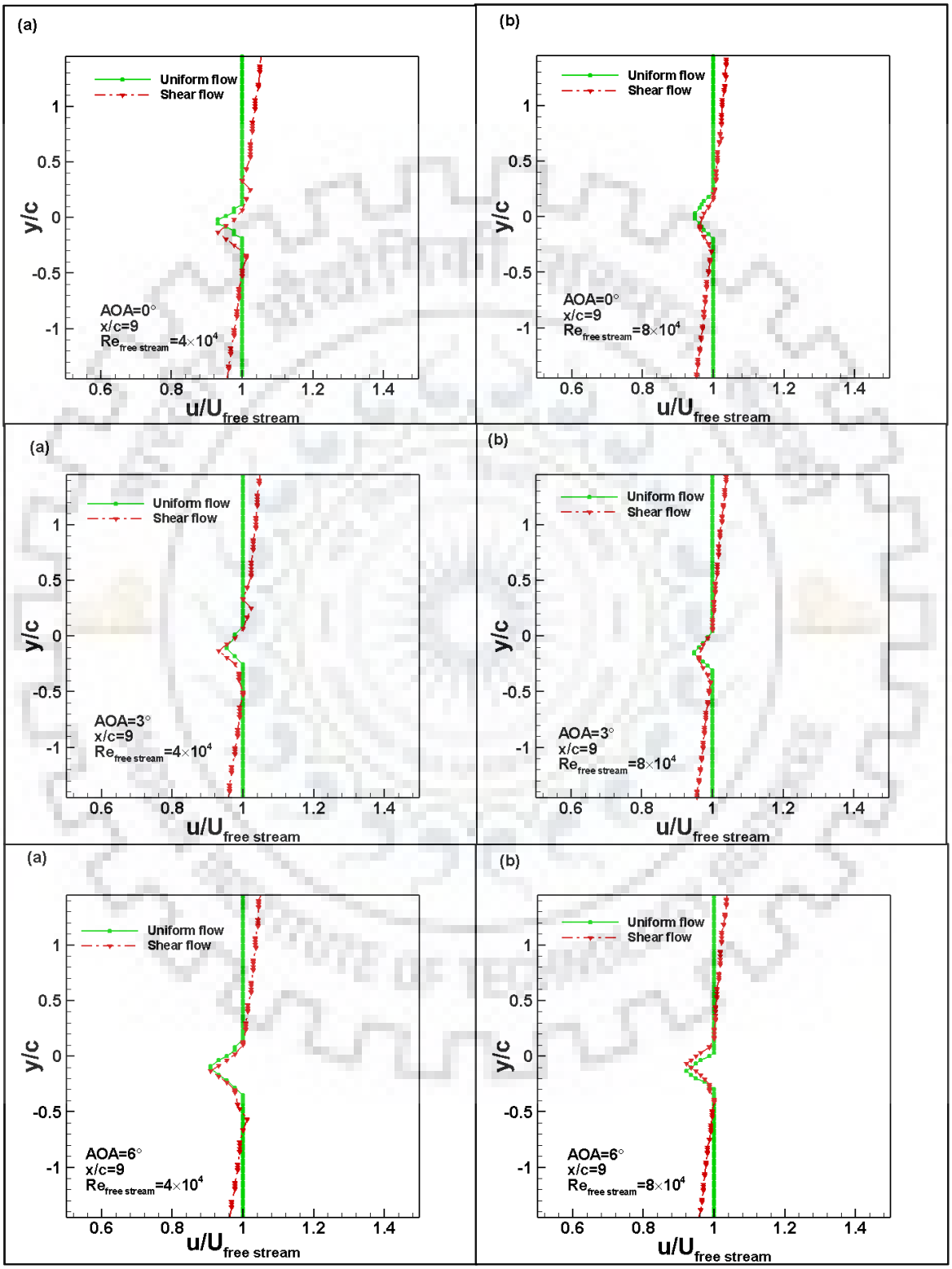

Fig. 5.18 Images of velocity profile far wake from the airfoil (measured with Pitot - static tube and Micro manometer) varying from 0º to 6º for both configurations.

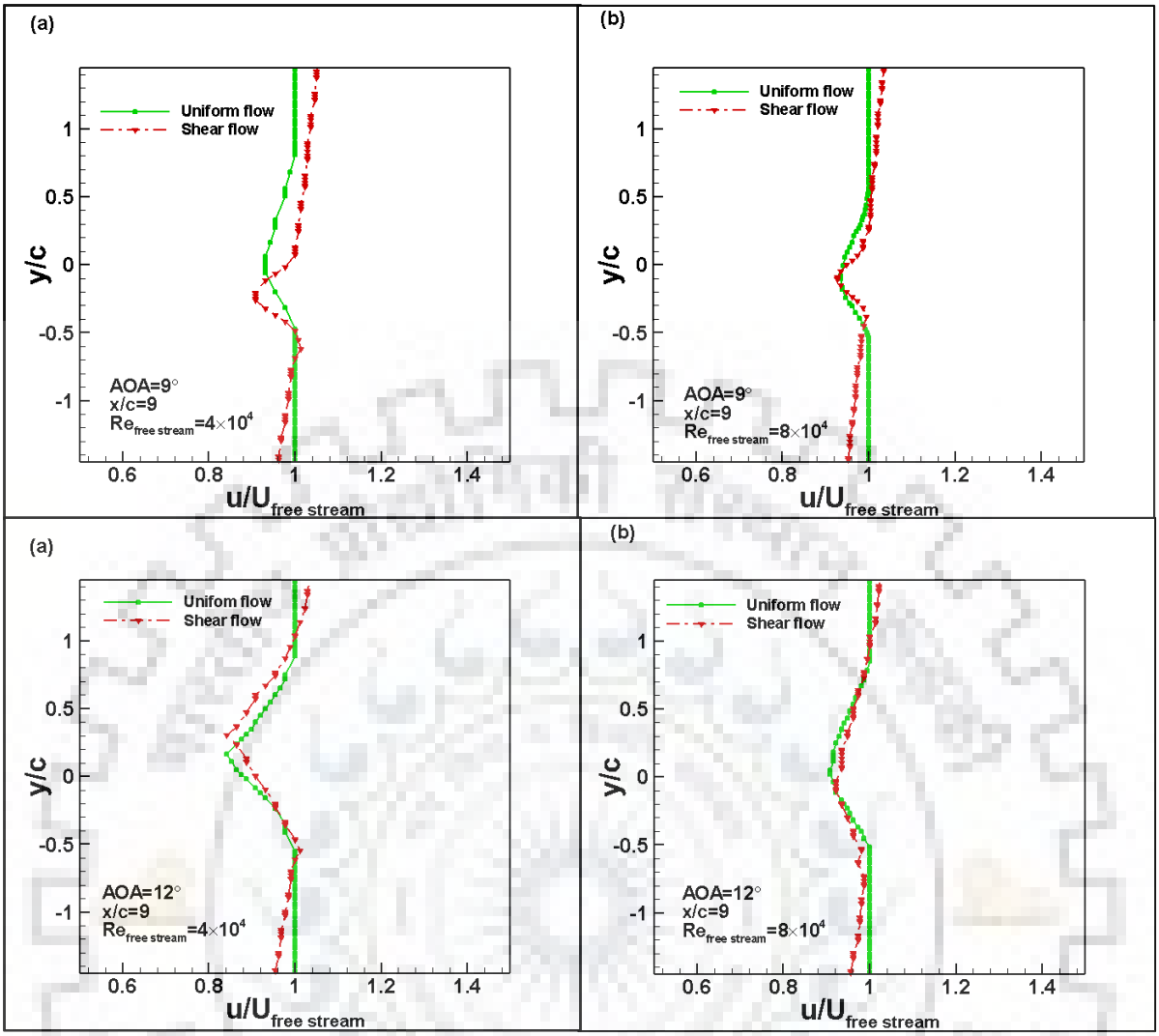

Fig. 5.19 Images of velocity profile far wake from the airfoil (measured with Pitot - static tube and Micro manometer) varying from 9º to 12º in the plane x/c=9 for both configurations.

In the plane x/c=9 for angle of attack of 0º to 6º the wake zone of shear inflow remains similar to the wake zone of uniform shear flow. For angle of attack of 9º for high Reynolds number this difference increases but for lower angle of attack this difference is significantly higher. For 12º of angle of attack wake width are similar for both Reynolds number but for high Re this wake zone shifts downward and for lower Re, this shifts in upward direction.

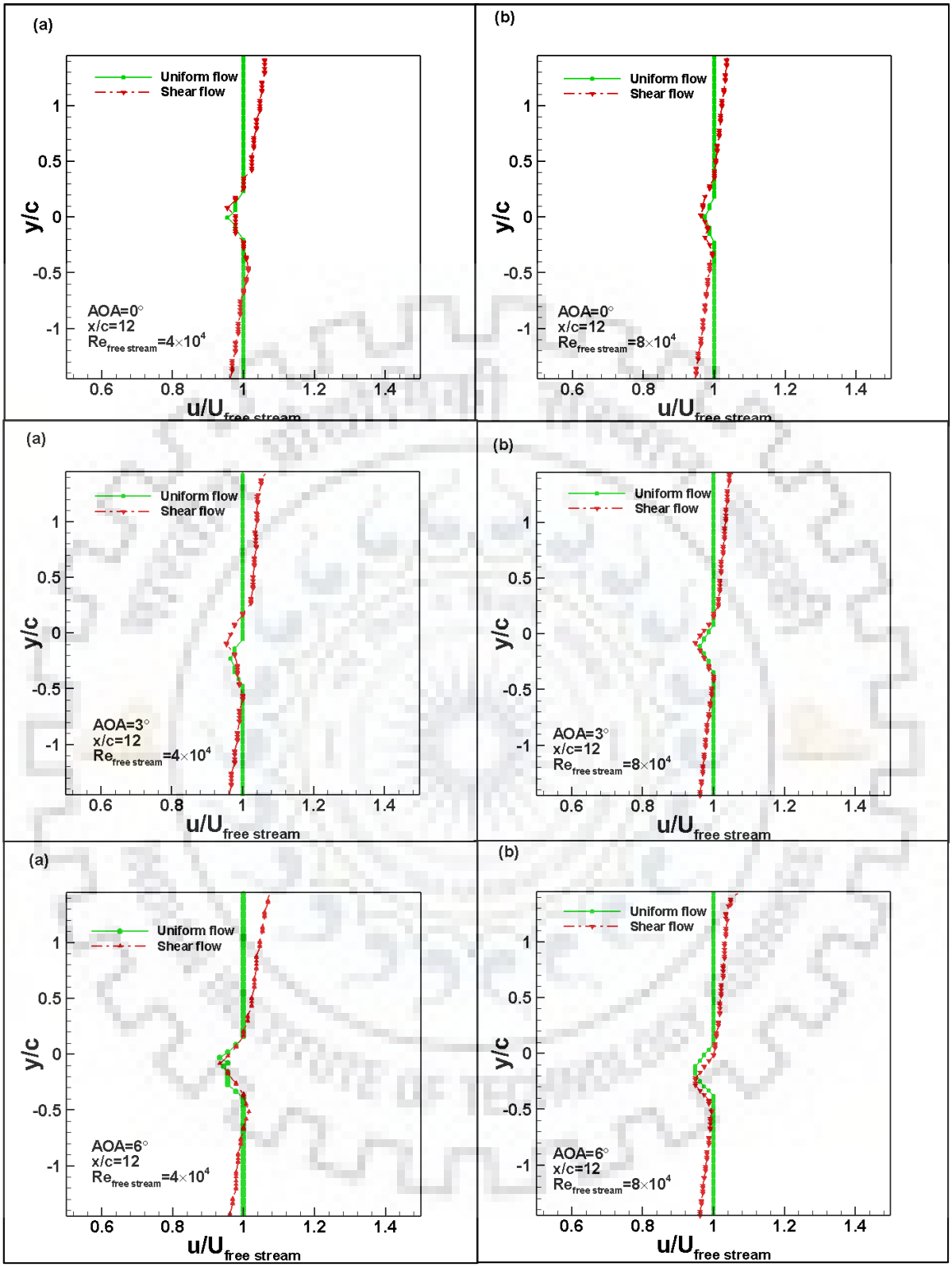

Fig. 5.20 Images of velocity profile far wake from the airfoil(measured with pitot-static tube and Micro manometer) varying from 0º to 6º in the plane x/c=12 for both configuration.

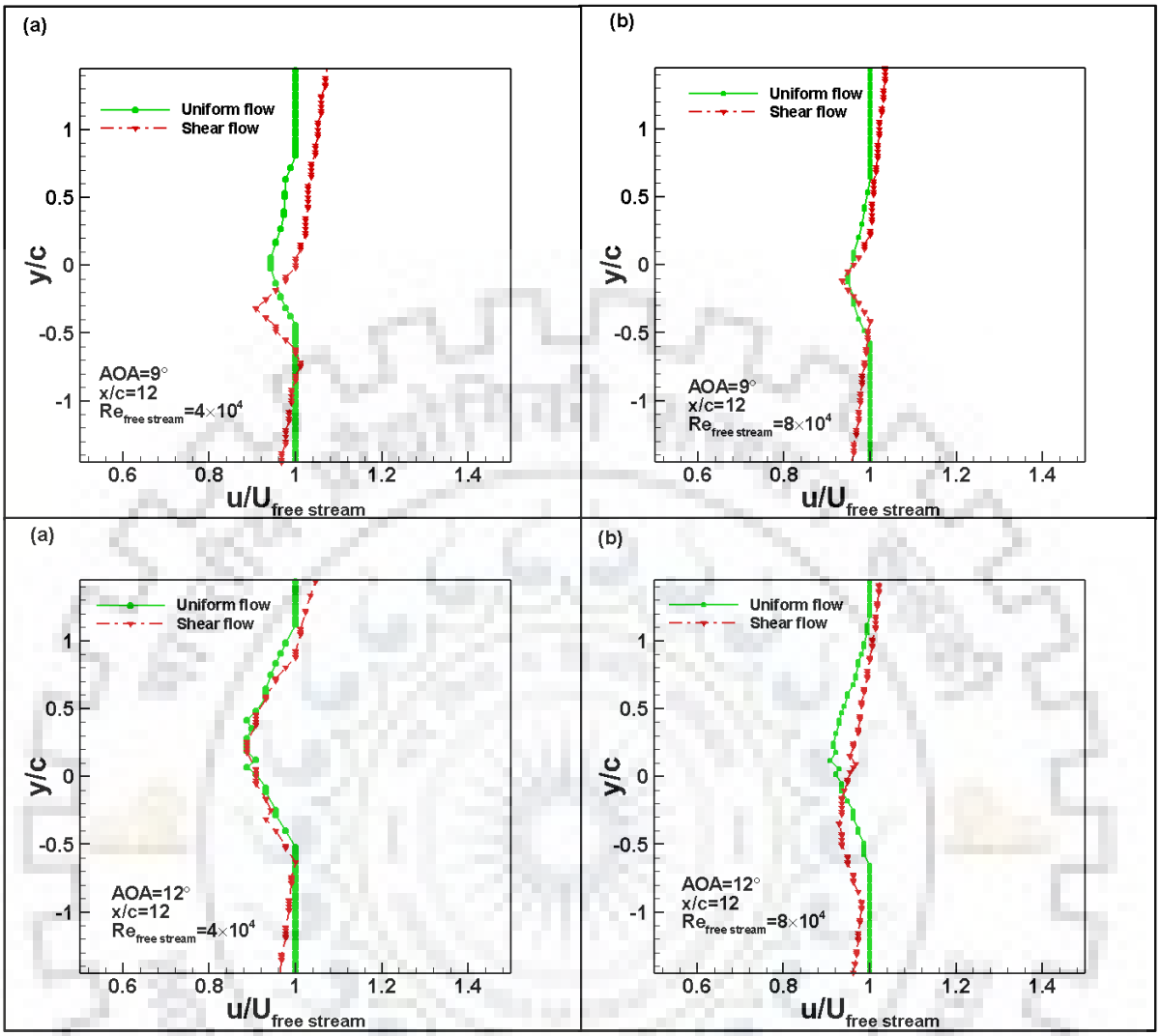

Fig. 5.21 Images of velocity profile far wake from the airfoil (measured with pitot-static tube and Micro manometer) varying from 9º to 12º in the plane x/c=12 for both configuration

For plane of x/c=12º the wake width difference increase compare to the plane x/c=9 similar downwaed shift was observed. At angle of attack of 9º for high Re the different wake profiele obtaine which was not obtaine for x/c=9. For high and low Re similar shiifting of wake zone obtained and also increase in velodeficite is marginabe same as in plane x/c=9.

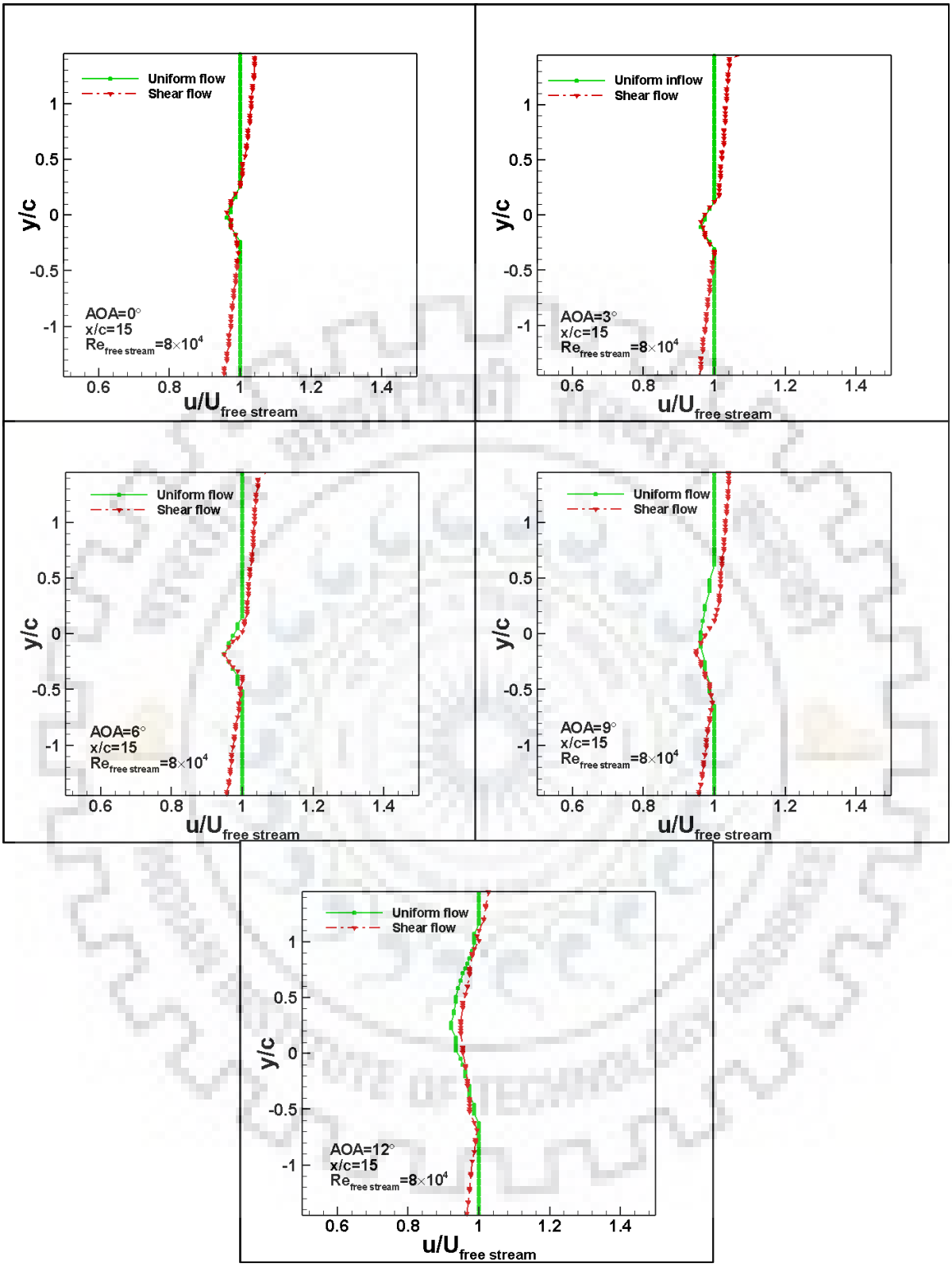

Fig. 5.22 Images of velocity profile far wake from the airfoil(measured with pitot-static tube and Micro manometer) varying from 0º to 12º in the plane x/c=15 for both configuration.

In x/c=15 for the lower Re the shear effect is weak hence no uniform shear profile obtained. Hence its plotting is not present here. For higher Re higher wake width in shear as well in uniform in flow is obtained compare to other two plane x/c=9 and x/c=12. Similar low wake width is obtained in angle of attack of 9º and shifting of wake in 12º angle of attack

5.7 Power spectrum

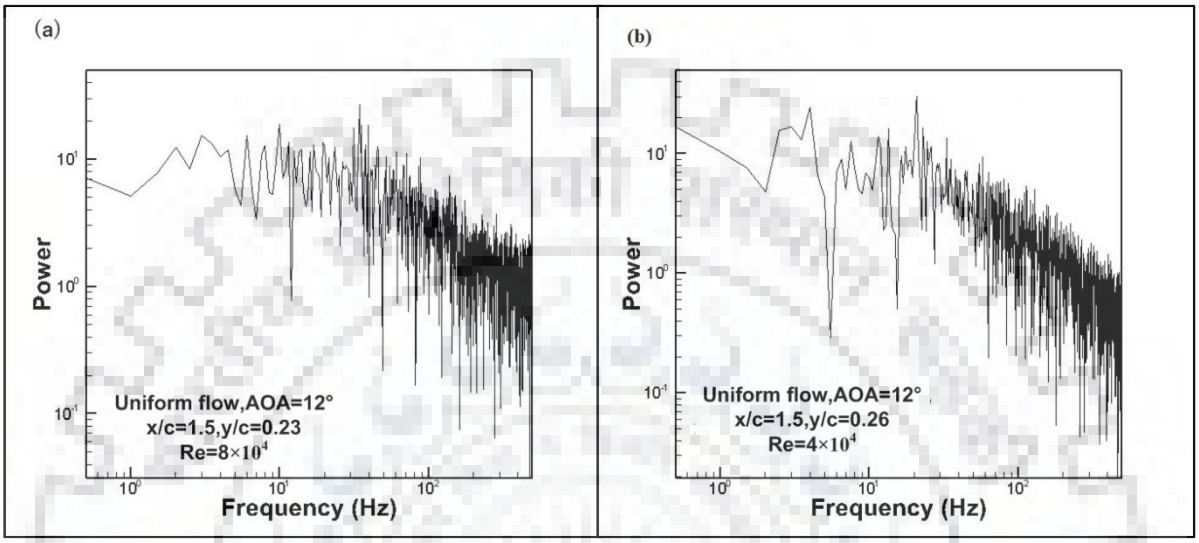

Fig. 5.23 power spectrum plot

Power spectra for few cases of uniform and shear inflow over the airfoil at high angles of attacks have been shown in figures 5.23, 5.24 and 5.25. Figure 5.23 shows the comparison of power spectrum for uniform inflow to the airfoil at AOA = 12º for the two Reynolds numbers under consideration in the present study. The peaks in the spectrum shows the vortex shedding frequency of the flow in their respective regimes. The downstream location is kept same for the comparison of the power spectra however the vertical location differs minutely. The figure clearly shows, increase in the vortex shedding frequency in higher Reynolds number case figure 5.23(b) with respect to lower Reynolds number flow case figure 5.23(a) which is obvious because of the increased inertia in the flow at higher Reynolds number.

Figure 5.24 shows the effect of AOA on vortex shedding frequency in the same flow regime for uniform inflow case. It shows that with decrease in AOA of the airfoil from 12º in figure 5.24(a) to degree to 9º in figure 5.24(b), there is a considerable decrease in the vortex shedding frequency of the flow over the airfoil. The reason behind this phenomenon can be explained in a way that with increase in the AOA. The airfoil behaves more with the bluff body characteristics and thus vortex shedding frequency increase is obvious.

Figure 5.25 compared the unsteady flow phenomenon of the case of uniform in figure 5.25(a) and shear in figure 5.25(b) inflow over the airfoil at higher Reynolds number 12º and . In the figure it can be seen that the vortex shedding frequency is decreased quite considerably with respect to uniform inflow case. The reason behind such finding can be the delay in the shear layer separation in the latter inflow case as elongated shear layers causes vortex shedding suppression in bluff body aerodynamics. At such high AOA the airfoil behaves as similar to bluff body.

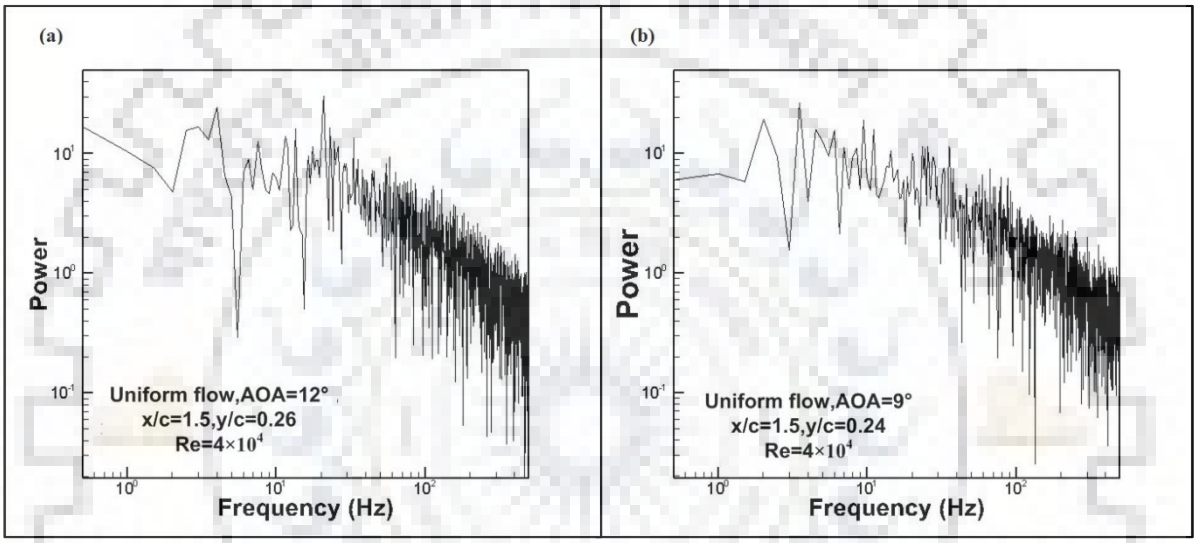

Fig.5.24 Power spectrum plot

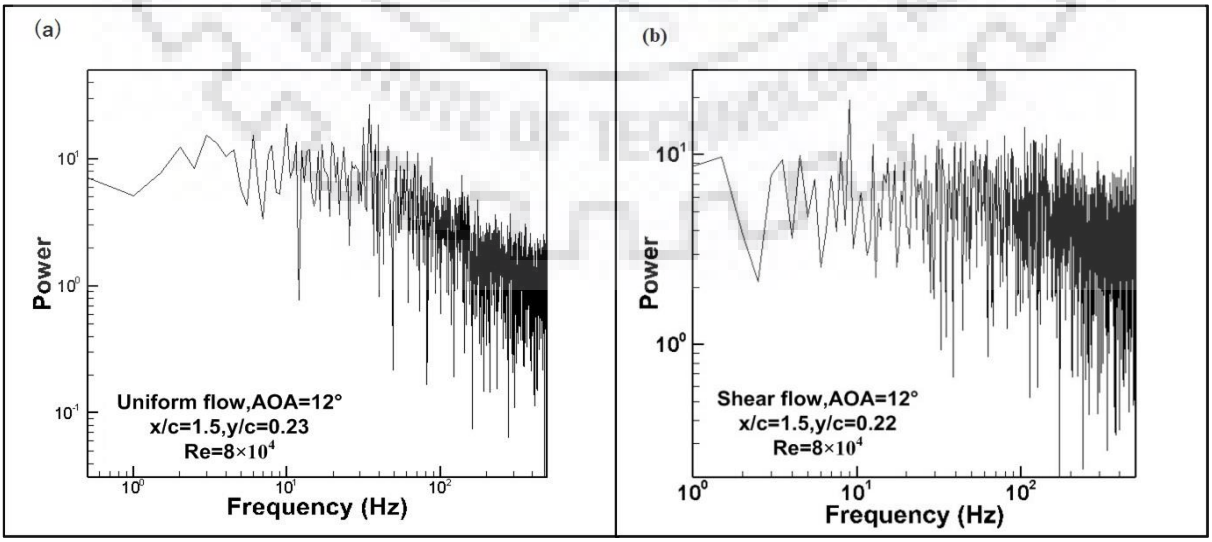

Fig. 5.25 Power spectrum plot

Chapter 6 Conclusions and Future Scope

Present study is an experimental investigation of effects of two different inflow conditions namely uniform free stream and uniform shear inflow over the NACA0012 airfoil. The experiments are performed in the subsonic open circuit wind tunnel. The shear screen is used to generate weak shear inflow condition prior to airfoil. CTA study is carried out to characterize the flow over the airfoil. Reading are taken at different downstream location over the suction surface of the airfoil as well as in the wake of the airfoil. Coefficient of drag is also evaluated in the far wake of the airfoil where static pressure variations in the flow are supposed to be minimum. Two Reynolds numbers (Re = 40,000 and 80,000) are considered in the study which belong to low Reynolds number regime. Five AOA are chosen in the study to see the effect of both inflow conditions on the unsteady wake and Drag characteristics of the airfoil. Here are few key findings of the study:

- Shear screen successfully generates the weak uniform shear flow downstream to it. The Shear parameter 'K' is found to be constant for both the Reynolds number considered in the study. The effect of this weak shear is found persistent up to x/c = 12 for low Reynolds number and x/c = 15 for high Reynolds number. So all the measurements are taken upstream of x/c = 12 location to avail the effect of uniform shear inflow over the airfoil.
- The turbulence intensity increases in comparison to uniform free stream flow condition, as the shear screen is imposed into the flow.
- For the uniform inflow condition, the vortex shedding is observed for AOA = 9º and 12º for both the Reynolds number.
- The velocity profiles obtained at different downstream locations over the suction surface of the airfoil show the boundary layer separation clearly which occurs in between x/c = 0 to 0.2 location for AOA = 6º and 9º, x/c = 0.2 to 0.4 for AOA = 12º for both the Re numbers.
- In the case of uniform shear inflow, the flow separation is noticed at x/c = 1, for AOA = 6º and 9º and in between x/c = 0.2 to 0.4 for AOA = 12º for both Re numbers. Clear delay in the flow separation can be noticed in the shear inflow case up to 9º AOA with respect to uniform shear inflow case for both Re numbers. The reason being the greater momentum in the boundary layer due to increased turbulence intensity in the flow. The

flow separation being unaffected for 12º AOA for both inflow conditions and both Re numbers.

- The drag coefficient is lower for shear inflow case with maximum reduction achieved for 9º AOA at both Re number by 69.49 % for low Re number and 42 % for higher Re number with respect to uniform free stream inflow case for both Re numbers and respective AOA.
- In the kinematic analysis of the flow it is found that the vortex shedding frequency for uniform free stream inflow case at 12º AOA is f_s = 22 Hz for Re = 40,000 and f_s = 30 Hz for Re = 80,000. Whereas, in the shear inflow case the vortex shedding frequency observed for 12º AOA is f_s = 10 Hz for high Re number.

The results obtained in the study show that uniform shear inflow enhances the flow characteristics of the airfoil better than uniform free stream flow by delaying the boundary layer separation and have greater efficacy to handle adverse pressure gradients at different AOA. The onset of vortex shedding is found only in high AOA in the shear inflow condition. Moreover, the drag coefficient is reduced for all AOA in the shear inflow case thus shows the improved load characteristics of the airfoil under shear inflow condition.

In the future scope of the study, the advanced flow diagnostic techniques like PIV and X-wire CTA measurements can be done for the same configurations. The flow visualization images can also be obtained in order to understand the flow physics involved and to compliment the PIV and CTA study.

References

1. Barbi, C., D. Favier, and C. Maresca. 1981. “Vortex Shedding from a Circular Cylinder in Oscillatory Flow.” *Unsteady Turbulent Shear Flows* 141: 248–1. https://doi.org/10.1007/978-3-642-81732-8_20.
2. Brendel, M., and T. J. Mueller. 1988. “Boundary-Layer Measurements on an Airfoil at Low Reynolds Numbers.” *Journal of Aircraft* 25 (7): 612–17. https://doi.org/10.2514/3.45631.
3. Cao, S., S. Ozono, K. Hirano, and Y. Tamura. 2007. “Vortex Shedding and Aerodynamic Forces on a Circular Cylinder in Linear Shear Flow at Subcritical Reynolds Number.” *Journal of Fluids and Structures* 23 (5): 703–14. https://doi.org/10.1016/j.jfluidstructs.2006.11.004.
4. Cao, Shuyang, Shigehira Ozono, Yukio Tamura, Yaojun Ge, and Hironori Kikugawa. 2010. “Numerical Simulation of Reynolds Number Effects on Velocity Shear Flow around a Circular Cylinder.” *Journal of Fluids and Structures* 26 (5): 685–702. https://doi.org/10.1016/j.jfluidstructs.2010.03.003.
5. Cao, Yong, and Tetsuro Tamura. 2018. “Shear Effects on Flows Past a Square Cylinder with Rounded Corners at Re=2.2×104.” *Journal of Wind Engineering and Industrial Aerodynamics* 174 (September 2017): 119–32. https://doi.org/10.1016/j.jweia.2017.12.025.
6. Chen, C. F. 1966. “Second-Order Theory for Airfoils in Uniform Shear Flow.” *AIAA Journal* 4 (10): 1712–16. https://doi.org/10.2514/3.3767.
7. Cheng, M., D. S. Whyte, and J. Lou. 2007. “Numerical Simulation of Flow around a Square Cylinder in Uniform-Shear Flow.” *Journal of Fluids and Structures* 23 (2): 207–26. https://doi.org/10.1016/j.jfluidstructs.2006.08.011.
8. Gad-el-Hak, Mohamed. 2008. “Micro-Air-Vehicles: Can They Be Controlled Better?” *Journal of Aircraft* 38 (3): 419–29. https://doi.org/10.2514/2.2807.
9. Ghorbanishohrat, F., F. Samara, and D. A. Johnson. 2016. “Investigation of Laminar Separation Bubble Behavior under Unsteady Flows Using PIV and Thermal Imaging Methods.” *18th International Symposium on the Application of Laser and Imaging Techniques to Fluid Mechanics*.
10. Hammer, Patrick R., Miguel R. Visbal, Ahmed M. Naguib, and Manoochehr M. Koochesfahani. 2018. “Lift on a Steady 2-D Symmetric Airfoil in Viscous Uniform Shear

Flow." *Journal of Fluid Mechanics* 837: R21–211. https://doi.org/10.1017/jfm.2017.895.

11. Hatman, A., and T. Wang. 2010. "A Prediction Model for Separated-Flow Transition." *Journal of Turbomachinery* 121 (3): 594. https://doi.org/10.1115/1.2841357.
12. Honda, M. 1960. "On Theory of Pulse Transmission in a Nerve Fibre Author (s): J . Engelbrecht Source : Proceedings of the Royal Society of London . Series A , Mathematical and Physical Published by : The Royal Society Stable URL : Http://Www.Jstor.Org/Stable/2990232." *JSTOR* 254 (1278): 372–94.
13. Hu, Hui, and Zifeng Yang. 2008. "An Experimental Study of the Laminar Flow Separation on a Low-Reynolds-Number Airfoil." *Journal of Fluids Engineering* 130 (5): 051101. https://doi.org/10.1115/1.2907416.
14. Huang, Rong F., and Chih L. Lin. 2008. "Vortex Shedding and Shear-Layer Instability of Wing at Low-Reynolds Numbers." *AIAA Journal* 33 (8): 1398–1403. https://doi.org/10.2514/3.12561.
15. James, D. G. 1951. "Two-Dimensional Airfoils in Shear Flow. I." *Quarterly Journal of Mechanics and Applied Mathematics* 4 (4): 407–18. https://doi.org/10.1093/qjmam/4.4.407.
16. Jones, Gareth, Matthew Santer, and George Papadakis. 2018. "Control of Low Reynolds Number Flow around an Airfoil Using Periodic Surface Morphing: A Numerical Study." *Journal of Fluids and Structures* 76: 95–115. https://doi.org/10.1016/j.jfluidstructs.2017.09.009.
17. Journal, Quarterly, O F Mechanics, T H E Effect, O F Wire, Gauze On, Small Disturbances, and I N A Uniform Stream. 1964. "The Effect of Wire Gauze on Small." *Victoria* 1 (1948).
18. Kang, S. 2006. "Uniform-Shear Flow over a Circular Cylinder at Low Reynolds Numbers." *Journal of Fluids and Structures* 22 (4): 541–55. https://doi.org/10.1016/j.jfluidstructs.2006.02.003.
19. Karnik, U., and S. Tavoularis. 1987. "Generation and Manipulation of Uniform Shear with the Use of Screens." *Experiments in Fluids* 5 (4): 247–54. https://doi.org/10.1007/BF00279737.
20. Kulkarni, Vinayak, Niranjan Sahoo, and Sandip D. Chavan. 2011. "Simulation of Honeycomb-Screen Combinations for Turbulence Management in a Subsonic Wind Tunnel." *Journal of Wind Engineering and Industrial Aerodynamics* 99 (1): 37–45. https://doi.org/10.1016/j.jweia.2010.10.006.
21. Kwon, Tae Soon, Hyung Jin Sung, and Jae Min Hyun. 2008. "Experimental Investigation

of Uniform-Shear Flow Past a Circular Cylinder." *Journal of Fluids Engineering* 114 (3): 457. https://doi.org/10.1115/1.2910053.

22. Kwon, T.S., Sung, H.J., Hyun, J.M. 1992. Experimental investigation of uniform-shear flow past a circular cylinder. *ASME Journal of Fluids Engineering* 114:457–460.
23. Kang, S. 2006. Uniform-shear flow over a circular cylinder at low Reynolds numbers. *Journal of Fluids and Structures, 22*(4): 541-555.
24. Laitone, E. V. 1997. "Wind Tunnel Tests of Wings at Reynolds Numbers below 70 000." *Experiments in Fluids* 23 (5): 405–9. https://doi.org/10.1007/s003480050128.
25. Lin, J. C. M., and Laura L. Pauley. 2008. "Low-Reynolds-Number Separation on an Airfoil." *AIAA Journal* 34 (8): 1570–77. https://doi.org/10.2514/3.13273.
26. Lissaman, P B S. 1983. "Low-Reynolds-Number Airfoils," 223–39.
27. Mallock, A. 2006. "On the Resistance of Air." *Proceedings of the Royal Society A: Mathematical, Physical and Engineering Sciences* 79 (530): 262–73. https://doi.org/10.1098/rspa.1907.0038.
28. Mueller, T. J., L. J. Pohlen, P. E. Conigliaro, and B. J. Jansen. 1983. "The Influence of Free-Stream Disturbances on Low Reynolds Number Airfoil Experiments." *Experiments in Fluids* 1 (1): 3–14. https://doi.org/10.1007/BF00282261.
29. Mueller, T J, S M Batill, and Notre Dame. 1980. "Experimental Studies of the Laminar Separation Bubble on a Two-Dimensional Airfoil at Low Reynolds Numbers." *AIAA 13th Fluid & Plasma Dynamics Conference*.
30. Mueller, Thomas J., and Stephen M. Batil. 1982. "Experimental Studies of Separation on a Two-Dimensional Airfoil at Low Reynolds Numbers." *AIAA Journal* 20 (4): 457–63. https://doi.org/10.2514/3.51095.
31. Nigam, L. N. 1963. "Constant Shear Flow Past an Airfoil with Arbitrary Surface Suction." *Applied Scientific Research, Section A* 11 (3): 225–44. https://doi.org/10.1007/BF03184982.
32. Ohtake, Tomohisa, Yusuke Nakae, and Tatsuo Motohashi. 2007. "Nonlinearity of the Aerodynamic Characteristics of NACA0012 Aerofoil at Low Reynolds Numbers." *Journal of the Japan Society for Aeronautical and Space Sciences* 55 (644): 439–45. https://doi.org/10.2322/jjsass.55.439.
33. Owen, P. R., and H. K. Zienkiewicz. 1957. "The Production of Uniform Shear Flow in a Wind Tunnel." *Journal of Fluid Mechanics* 2 (06): 521. https://doi.org/10.1017/s0022112057000336.
34. Rohr, J. J., E. C. Itsweire, K. N. Hellandii, and C. W. Van Atta. 1988. "An Investigation

of the Growth of Turbulence in a Uniform-Mean-Shear Flow." *Journal of Fluid Mechanics* 187: 1–33. https://doi.org/10.1017/S002211208800031X.

35. V Somashekar, and A. Immanuel Selwyn Raj. 2018. "Experimental Investigation on Laminar Separation Bubble Over an Airfoil a Review." *Indian Journal of Science and Technology* 11 (11): 1–9. https://doi.org/10.17485/ijst/2018/v11i11/119288.
36. Sturm, Hannes, Gerrit Dumstorff, Peter Busche, Dieter Westermann, and Walter Lang. 2012. "Boundary Layer Separation and Reattachment Detection on Airfoils by Thermal Flow Sensors." *Sensors (Switzerland)* 12 (11): 14292–306. https://doi.org/10.3390/s121114292.
37. Sumner, D., and O. O. Akosile. 2003. "On Uniform Planar Shear Flow around a Circular Cylinder at Subcritical Reynolds Number." *Journal of Fluids and Structures* 18 (3–4): 441–54. https://doi.org/10.1016/j.jfluidstructs.2003.08.004.
38. Tsien, hsue-shen. 1943. "symmetrical joukowsky airfoils in shear flow author (s): hsue-shen tsien source : quarterly of applied mathematics , vol . 1 , no . 2 (july , 1943), pp . 130-148 published by : brown university stable url : http://www.jstor.org/stable/43633399 accesse." *Jstor* 1 (2): 130–48.
39. Tsuchiya, Takaaki, Daiju Numata, Tetsuya Suwa, and Keisuke Asai. 2013. "Influence of Turbulence Intensity on Aerodynamic Characteristics of an NACA 0012 at Low Reynolds Numbers," no. January: 1–15. https://doi.org/10.2514/6.2013-65.
40. Watkins, S., S. Ravi, and B. Loxton. 2010. "The Effect of Turbulence on the Aerodynamics of Low Reynolds Number Wings." *Engineering Letters* 18 (3).
41. Winslow, Justin, Hikaru Otsuka, Bharath Govindarajan, and Inderjit Chopra. 2017. "Basic Understanding of Airfoil Characteristics at Low Reynolds Numbers (104–105)." *Journal of Aircraft* 55 (3): 1050–61. https://doi.org/10.2514/1.c034415.
42. Yarusevych, Serhiy, Pierre E. Sullivan, and John G. Kawall. 2009. "On Vortex Shedding from an Airfoil in Low-Reynolds-Number Flows." *Journal of Fluid Mechanics* 632: 245–71. https://doi.org/10.1017/S0022112009007058.